A distributed wind downscaling technique for wave climate modeling under future scenarios

Mohamad Javad Alizadeh[1*], Mohamad Reza Kavianpour[1], Bahareh Kamranzad[2,3], Amir Etemad-Shahidi[4]

[1]Faculty of Civil Engineering, K.N.Toosi University of Technology, Tehran, Iran
Corresponding author's email: mjalizadeh@mail.kntu.ac.ir

[2]Graduate School of Advanced Integrated Studies in Human Survivability (GSAIS), Kyoto University, Yoshida-Nakaadachi 1, Sakyo-ku, Kyoto 606-8306, Japan

[3]Hakubi Center for Advanced Research, Kyoto University, Yoshida Honmachi, Sakyo-ku, Kyoto, 606-8501, Japan

[4]Griffith School of Engineering and Built Environment, Griffith University, Gold Coast, 4222, Australia

Abstract: The aim of this study is to develop a Weibull-based distributed downscaling technique for wind field as forcing for the wave models to investigate the wave climate under future scenarios. For this purpose, the statistical downscaling approach modifies Weibull distribution parameters of the global circulation model wind speeds based on the corresponding features of wind data of ECMWF (European Center for Medium-Range Weather Forecasts). The proposed technique has the advantage of modifying the wind components in each grid point based on the corresponding values in the same grid point of ECMWF wind field. Hence, it is superior to other existing models due to considering the spatial variation. The previous models using inverse distance weighting suffer from heterogeneity and ignoring spatial variation in areas with high gradient of wind speed. Moreover, the Weibull-based technique outperforms the existing statistical downscaling techniques in terms of accuracy. Prior to investigate future distribution of wave characteristics, performance of the selected GCM was evaluated and compared against the corresponding models obtained from the available regional climate models. Future projections of wind fields (RCP4.5, RCP8.5) were downscaled for the period of 2081 to 2100 with the proposed model as driving force for wave modeling in the Persian Gulf. To investigate the impacts of climate change on wave characteristics, results of the wave simulations from a third generation wave model (SWAN) for future scenarios are compared with those of the historical period (1981-2000) in monthly, seasonal, and annual scales. Generally, for RCP8.5, the results indicate a decrease in future significant wave height and peak wave period about 15% and 5%, respectively. However, the change of wave direction is marginal. Moreover, wave models forced with RCP4.5 wind data provide slightly higher average values in terms of wave height and peak wave period compared to those of RCP8.5.

Keywords: Wave climate, Future scenarios, Climate change, Distributed downscaling approach, Wind field, Weibull parameters

1. Introduction

Ocean surface gravity waves generated by the wind action over air-sea interface (henceforth called waves) contain more than half of the energy carried by all waves at the ocean surface surpassing the contribution of tides, tsunamis, coastal surges, and others (Semedo et al., 2011). They are of great importance for many different coastal engineering applications such as design and construction of coastal protection structures and harbors, marine transportation, sediment transport studies, coastal geomorphology and environmental purposes. Wave climate can refer to distribution of wave characteristics (e.g., height, period, and direction) for a given place averaged over several years. Therefore, investigation of wave climate is a key element toward reliable design and development of coastal and marine industries.

Climate change and its impacts on a variety of atmospheric, oceanic and earth surface processes have taken much attention, and several different general circulation models (GCMs) considering different scenarios and future probable conditions have been run in order to generate the projection of different variables. Thus, due to existing outputs of several GCMs representing climate change and global warming influences on different variables which the planet is experiencing, consideration of future trends in wave climate is an essential step for operation and designing of offshore and onshore structures. Recently, regional climate models (RCMs) considering the regional conditions have been developed to overcome coarse resolution of the GCMs. In this regard, CORDEX (Coordinated Regional Climate Downscaling Experiment) outputs are among the most popular RCMs available for climate change studies for different regions over the world. However, little attention was devoted for projection of wind waves in the Intergovernmental Panel on Climate Change (IPCC) Coupled Model Intercomparison Project Phase 5 (CMIP5). On the other hand, surface winds have received more attention and subsequently, they have been simulated and presented as outputs of several GCMs/RCMs under different future scenarios. Since the surface winds are considered as the main driving forces for wind waves, they can be employed in wave models to project wave climate under different climate change conditions. In this regard, many researchers applied wind data from different GCMs for investigation of wave characteristics and its prospective changes (Hemer et al., 2013b; Kamranzad et al., 2015; Semedo et al., 2018; Vanem, 2015; Wandres et al., 2017; Wang et al., 2018).

Semedo et al. (2012) employed a global wave model to explore impacts of future warmer climate through A1B emission scenario. The results indicated increasing and decreasing trends in mean significant wave height (H_s) for lower and higher latitudes, respectively. The variations are more intensified in southern hemisphere compared to the northern one. Hemer et al. (2013a) reported a decrease in annual mean H_s over 25.8% of the global ocean area whereas a projected increase in annual mean H_s was found over 7.1% of the global ocean predominantly in the Southern Ocean. Moreover, it was shown that the decrease rate is greater during boreal winter than austral winter, while the increase rate is greater for austral winter. Wang et al. (2015) investigated a 20-model ensemble of H_s simulations for the period 2006– 2099. The results revealed that the model

uncertainty is about 10 times as large as the variability between the RCP4.5 and RCP8.5 scenarios. Ruest et al. (2016) investigated the effect of sea ice on wave climate in The Gulf of St. Lawrence, Canada. The results implied that extreme H_s on the Gulf decreased during 1981 to 2010 due to effect of sea ice. However, for future climate condition and because of reduction of sea ice and its impacts on the Gulf climate, an increase in extreme wave height was predicted. Hegermiller et al. (2017) and Camus et al. (2017) applied multimodal wave spectrum technique for statistical downscaling of local wave climate by using the relationship between sea level pressure (SLP) and wave parameters. The results demonstrated efficiency of the proposed methods to statistically model multimodal wave climate. Wandres et al. (2017) investigated future prospective of wave energy along southwestern Australia under RCP4.5 and RCP8.5 scenarios. The results indicated an increase up to 20% in mean wave energy flux in shallow waters under both future scenarios. Moreover, it was found that changes in offshore mean wave direction have more impacts on nearshore and shelf wave climate compared to wave height in offshore. Aarnes et al. (2017) projected a decreasing trend in annual mean significant wave height in the northeast Atlantic under future climatic conditions. According to their study, it can be found that both scenarios (RCP4.5 and RCP8.5) projects the largest changes in significant wave height around the mean while for the upper tail of the distribution the tendency is weaker. However, for the extremes, an increase was reported in some locations such as west of the British Isles and the southern coastal areas of Norway. Casas-Prat et al. (2018) employed WAVEWATCH III and GCM data of sea ice and wind (RCP8.5) to project global ocean wave climate. The study demonstrated a decrease in wind speed and wave height in the North Atlantic and an increase in annual mean of wind speed, wave height and peak wave period in mid-high latitudes of the Sothern Hemisphere. Moreover, a significant counterclockwise rotation in the mean wave direction was projected in the Southern Hemisphere which resulted in more intense waves travelling towards the Equator and developing into swells. This can be considered as the main reason for increasing trends in wave height and period in the East Pacific and Indian Oceans while a decreasing pattern for wind speeds are projected for these areas. A similar trend for variation in global ocean wave climate in the mid-21st century (2013-2060) has been reported in a separate research study by Lemos et al. (2019). For this purpose, WAve Model (WAM) forced with outputs of ice coverage and wind speed from EC-Earth projections under RCP8.5 was employed to simulate wave climate for future warmer climate.

Global wave climate projection is beneficial to investigate general trends in future conditions, while for practical applications in coastal engineering, simulating wave climate at local scale is of great importance to extract more details with higher accuracy and reliability for a particular area. In this regard, wave models forcing with localized GCM (downscaled) wind data are an appropriate proxy to investigate the change of wave climate under future projections. Generally speaking, the GCMs are normally run for globally scale and represent coarse resolution which can not reflect topographical effects. Therefore, it is a common task to downscale GCM outputs prior to driving wave models. Previously, dynamical and statistical downscaling techniques have been employed for this purpose with the latter one attracting much popularity due to its

simplicity and easy application. To project future wave climate, statistical techniques using regression models are employed to make a relationship between predictors including atmospheric variables (such as surface wind speed, mean sea level pressure, etc.) and ocean wave heights as predictant (Caires et al., 2006; Wang et al., 2014; Wang et al., 2010). It was indicated that using surface wind speed alone as the most important predictor might be sufficient to represent ocean wave heights even though other variables such as anomalies of sea level pressure can be considered as supplementary predictors to make improvement on the predictant estimation (Wang et al., 2010). Thus, different types of statistical techniques such as quantile mapping (QM), multiplicative shifting method (MSM), and machine learning based models were developed to downscale atmospheric variables such as wind speed/components for a given point or station (Breslow and Sailor, 2002; Kamranzad et al., 2015; Sangelantoni et al., 2018). Regardless of the statistical downscaling type, the previous models were usually implemented based on inverse distance weighting which does not consider the spatial distribution for regions with rapid changes in wind speeds. Therefore, development of distributed downscaling models which reflect spatial characteristics of the climatic variable is of great interest for future wind and wave projections.

The aim of this study is to develop a robust distributed downscaling approach for the wind field to be used as the forcing for wave models and to investigate the wave climate under future projections. The model is established by modifying Weibull parameters of simulated wind components obtained from GCM at each grid cell and repeating the process for the other cells in the domain. It has two advantages of 1) the distributed feature consider spatial variation of the variable is superior to inverse distance weighting already applied for downscaling purpose, 2) the Weibull method yields better predictions than existing regression based techniques. Additionally, performance of different GCMs and also three different regional climate models (RCMs) are evaluated to select the best climatic model providing wind data for wave model development. Eventually, the modified GCM wind fields are used as forcing for the SWAN model to simulate the wave climate in the Persian Gulf. In section 2, study area, data resources and methodology are described. Results related to wind speed projection and changes in wave climate in monthly, seasonal and annual scales are discussed in section 3. Main findings of the study are summarized in the last section.

2. Materials and methods

2.1. Study area and data resources

The Persian Gulf, as a semi-enclosed crescent-shape sea, is an extension of the Indian Ocean that runs northwest of the Gulf of Oman, surrounded by the Iranian Plateau in the north and the Arabian Peninsula in the south (Figure 1). The narrowest part of the Persian Gulf (called the Strait of Hormuz) links it to the open ocean. Due to having the largest oil resources in the world, fishing ground, reefs and oysters, the Persian Gulf has a great importance for industrial,

economic and ecological aspects. Study of wave climate and its future changes in the Persian Gulf is beneficial for many purposes such as development of marine industries, transportation, port design and operation, and coastal structures. The so-called Shamal wind is the dominant wind in the area affecting middle and northwestern parts of the Persian Gulf which mainly blows in summer and winter seasons. To investigate the wave climate in the study area, 4 points in different parts of the Persian Gulf have been considered as the selected stations (Figure 1). Table 1 summarizes the geographic coordinates and depths of the selected stations.

Figure 1. Study area and selected stations

Table 1. Location and depth of the selected stations

Point	Long.	Lat.	Label	Depth
1	50.67	28.7875	*W*	28.6
2	52.50	27.3180	*M1*	64.9
3	56.20	26.5000	*E*	82.5
4	53.00	25.6000	*M2*	37.2

The datasets used in this study include ECMWF ERA-Interim reanalysis wind data (Dee et al., 2011) for the period of 1981 to 2000 as reference wind data, and historical (1981-2000) and future (2081-2100) GCM wind data. There are many different GCMs/RCMs providing the wind outputs for future scenarios in which the appropriate one should be selected having the highest consistency with the wind climate of the area. In this regard, outputs of two different GCMs of CMCC-CM and MPI-ESM-LR and CORDEX outputs of three RCMs of EC-EARTH, CNRM and GFDL-ESM2M have been assessed prior to wave future projection. The CORDEX outputs of MENA (Middle East and North Africa) were employed to cover the study area properly. Table 2 gives characteristics of different climate models considered as tentative wind data for wave simulations.

Table 2. Characteristics of the GCMs/RCMs

GCM/RCM	Name	Institute	Resolution	
			Spatial (degree)	Temporal
GCM	CMCC-CM	The Centro Euro-Mediterraneo sui Cambiamenti Climatici Climate Model	0.75×0.75	3hr
GCM	MPI-ESM-LR	Max Planck Institute	1.865×1.875	3hr
RCM	EC-EARTH	European community Earth-System Model	0.22×0.22	1day
RCM	GFDL-ESM2M	The Geophysical Fluid Dynamics Laboratory	0.22×0.22	1day
RCM	CNRM-CM5	Centre National de Recherches Meteorologiques	0.44×0.44	1day

There are many different GCMs that provide wind data for historical and future scenario with different spatial and temporal resolution. Exploring efficiency of other GCMs for the study area to select the best GCM can be interesting although it could be expected that these differences are smaller in the corrected data (downscaled data). Abbasian et al. (2019) evaluated performance of 37 different GCMs of CMIP5 in simulating temperature and precipitation over Iran indicating efficiency of CMCC model for climate projection in the area. Similarly, results of the other studies revealed that the CMCC is among the best GCMs representing climatic variable over the north-east Atlantic region (Perez et al., 2014), India (Mishra et al., 2014), and Pakistan (Khan et al., 2018). However, applying ensemble models gaining advantage of several GCMs can be a good option to deal with uncertainty embedded in GCMs than running the model for a single GCM (Hemer et al., 2013a; Wang et al., 2015). The primary purpose of this study was to apply the proposed downscaling approach for the CMCC-CM model representing higher spatial and temporal resolution than the other GCM. However, efficiency of the other GCM and RCMs (Table 2) has been investigated to demonstrate suitability of the selected climate model. The future GCM outputs have been obtained by running global circulation models using different assumption of greenhouse gas concentration scenarios known as the Representative Concentration Pathways (RCPs) in which, RCP4.5 (an intermediate concentration scenario) and RCP8.5 (a high concentration scenario) are two commonly studied scenarios. RCP4.5 and RCP8.5 describe scenarios with radiative forcing reaching 4.5 W/m^2 and 8.5 W/m^2 respectively, by the end of the year 2100. All utilized datasets were retrieved with 0.75°×0.75° and 6 hourly spatial and temporal resolutions, respectively. Moreover, both ECMWF (ERA-Interim) and CMCC-CM (historical and RCPs 4.5 and 8.5) have single ensemble member size. Due to lower temporal resolution of ECMWF wind data (6 hr), the GCM data were applied with 6 hr intervals even though the datasets were available for finer resolution (3 hr). Formerly, ECMWF wind data have been successfully applied for assessment of wind and wave climate in different areas (Amirinia et al., 2017; Kamranzad et al., 2016; Kamranzad et al., 2015; Patra and Bhaskaran, 2017; Wandres et al., 2018). It is noticed that wind data with higher resolution are desirable for such a study area to reflect land-sea effects. However, lack of data with required resolution is a big limitation for this purpose. Using ERA-Interim wind data to force SWAN model in the North Atlantic, it was found that a coarse resolution wave model may give a few meters lower extreme H_s than a high resolution model (Bitner-Gregersen et al., 2016). Figure 2 illustrates the spatial distribution of average wind speeds of ECMWF and GCM in the study area from 1981 to 2000. As observed from Figure 2, the wind speed has higher averages in the middle and northwestern parts of the Persian Gulf which can reflect the impact of the Shamal Wind. Although there are some inconsistencies in wind speed pattern in outer part of the Persian Gulf, the spatial variation of wind speed for both data resources shows roughly a similar pattern. Generally, for the study area, it can be stated that the GCM wind speed has lower averages than the corresponding values of ECMWF. However, the GCM outputs due to running on a global scale may ignore topographical and land-sea interface effects.

Figure 2. Spatial distribution of wind speed in historical period a) ECMWF b) GCM

2.2. Wind modification and downscaling

2.2.1. Weibull-based technique

Downscaling of GCM wind outputs using different statistical techniques is a common task dealing with climate change studies. Thus, many different techniques such as nonlinear and linear regressions, quantile mapping, Weibull based approach and artificial intelligence methods have been employed to diagnose the relationship between the GCM outputs as predictor with those of reference data as predictand. Goly et al. (2014) and Shirkhani et al. (2015) showed that regression models perform poorly when applied for downscaling purpose of precipitation and wind speed. Moreover, they indicated superiority of quantile mapping and support vector methods over linear and nonlinear regression based models. Alizadeh et al. (2019) indicated that Weibull based model outperforms the support vector regression, quantile mapping and delta methods for wind downscaling. However, it is readily acknowledged that considering different existing statistical downscaling techniques is not in the scope of this study. From a preliminary investigation and based on the literature it can be understood that the wind speed usually follows a Weibull distribution (Shin et al., 2018). Therefore, gaining this characteristic of wind data can be deemed as a sufficient way to match the distribution between predictand and predictor. Moreover, previous studies confirmed successful applications of different variant of Weibull methods for wind downscaling (Chang et al., 2015; Tye et al., 2014). Generally, a Weibull distribution is described with two parameters: shape (k) and scale (A), which represent the peakedness and mean of the distribution, respectively. The distribution is also called Rayleigh when the shape parameter reaches 2. As the Weibull distribution can be only fitted on positive values while the ECMWF and GCM wind data contains both negative and positive values, the datasets were transformed to positive values before implementation the downscaling process. The probability density function (PDF) of Weibull distribution can be written as:

$$f(V) = \frac{k}{A}\left(\frac{V}{A}\right)^{k-1}\exp\left[-\left(\frac{V}{A}\right)^{k}\right] \quad (1)$$

where V represents eastward/northward wind speed. The Weibull parameters of A and k can be obtained through the maximum likelihood estimation as the following iterative equations (Chang et al., 2003):

$$k = \left(\frac{\sum_{i=1}^{n} V_i^k \ln(V_i)}{\sum_{i=1}^{n} V_i^k} - \frac{\sum_{i=1}^{n} \ln(V_i)}{n}\right)^{-1} \quad (2)$$

$$A = \left(\frac{1}{n}\sum_{i=1}^{n} V_i^k\right)^{1/k} \quad (3)$$

where n is the number of samples and V_i is the wind speed in time stage i.

To begin the downscaling process, firstly the Weibull parameters are computed for historical ECMWF and GCM wind components. Afterwards, the difference in historical period and with stationary assumption is added to the Weibull parameters calculated for the future scenarios. Finally, by fitting an inverse Weibull function to the probabilities, the wind data are extracted and subsequently de-transformed to their original ranges.

2.2.2. Quantile mapping (QM) approach

The QM approach aims to match the cumulative distribution functions (CDF) of GCM wind data to those of observed or reference data (here it means ECMWF wind data). It has been widely employed for downscaling purpose of climatic variables such as wind speed, temperature, and precipitation. The stationary assumption is also used for QM approach and the difference between wind speed of ECMWF and GCM during historical period is imposed on the cumulative distribution function of wind data for future scenario (Themeßl et al., 2012). The assumption is a common task dealing different statistical downscaling techniques even though it can add uncertainty on future climate projections. It has been discussed in details in Dixon et al. (2016). In brief, the method can be mathematically formulated as:

$$V_{GCM^{fut,\,corrected}_{i}} = V_{GCM^{fut}_{i}} + R_i \quad (4)$$

where i stands for the month and R_i is given as follows:

$$R_i\left[cdf_{V_{GCM^{fut}_{i}}}\left(V_{GCM^{fut}_{i}}\right)\right] = cdf^{-1}_{V_{ECMWF^{his}_{i}}}\left[cdf_{V_{GCM^{fut}_{i}}}\left(V_{GCM^{fut}_{i}}\right)\right] - cdf^{-1}_{V_{GCM^{his}_{i}}}\left[cdf_{V_{GCM^{fut}_{i}}}\left(V_{GCM^{fut}_{i}}\right)\right] \quad (5)$$

where cdf and cdf^{-1} are empirical cumulative distribution function and inverse empirical cumulative function, respectively. For more details about the approach, one can refer to the related literature (Li et al., 2010; Themeßl et al., 2012).

2.2.3. The proposed distributed model

To investigate the wave climate under future climatic scenarios for a given area, it is necessary to adopt coarse resolution of GCM wind data into local characteristics of the wind climate. This task is usually carried out by applying inverse distance weighting approach (Burrough and McDonnell, 1998; Kamranzad et al., 2015). In other words, for a particular region, some grid points are selected as representative points and the other grid points are modified based on their

distance from adjacent selected points. The main disadvantage embedded the approach is that it does not reflect spatial distribution of locations with high gradient in wind speed or the topographical effects. To overcome this problem, this study introduces and applies a new distributed Weibull-based model in which the GCM wind data are modified (in each grid point) based on the corresponding values (observed/reanalysis data) of the same grid point. Assuming ECMWF wind data as reference data for modification of GCM wind data for future scenarios, the main steps toward development of the proposed model can be summarized as follows (Alizadeh et al., 2019):

1- Collocate wind data of ECMWF with the GCM outputs and also transform the dataset to positive values (adding the absolute value of the minima of the wind data for each grid point).
2- Compute the difference between Weibull parameters of ECMWF with those of GCM during historical period.

$$D_{k(i)} = k_{ECMWF}^{his} - k_{GCM}^{his} \quad (6)$$

$$D_{A(i)} = A_{ECMWF}^{his} - A_{GCM}^{his} \quad (7)$$

where D_k,D_A are difference in shape and scale parameters of Weibull distribution, respectively. $i = 1...12$ represents the month.
3- Modifying the Weibull parameters obtained for GCM future scenarios as:

$$k'^{fut}_{GCM(i)} = k_{GCM(i)}^{fut} + D_{k(i)} \quad (8)$$

$$A'^{fut}_{GCM(i)} = A_{GCM(i)}^{fut} + D_{A(i)} \quad (9)$$

where k' and A' are the modified shape and scale parameters of the GCM wind speeds for a given future scenario.

4- Extract wind components by fitting an inverse Weibull function but with modified Weibull parameters.
5- Bringing the data to their original range by de-transformation (subtracting the added values in the transformation stage).
6- Repeating this procedure for all grid points in the computational domain (this step reflects the distributed feature of the method).

It is noticed that the Weibull distribution based technique does not disrupt temporal sequence of the downscaled time series. In other words, the temporal sequence of the model outputs will remain the same as the original dataset. Due to high values of shape parameter (k>2) for the transformed data of wind components, the distribution has two tails. These two tails can give the negative and positive extremes if wind data following an inverse Weibull function and de-transformation process. Through the data transformation, the data representing calm state are shifted forward in which during de-transformation they will be shifted backward retrieving their

original range. To implement this process, a *MATLAB* code has been developed in which the GCM outputs related to surface wind components under future scenarios are modified based on Weibull parameters (see Appendix A for details).

2.3. Numerical wave modelling

The SWAN (Simulating Waves Nearshore) wave model (Booij et al., 1999) was forced by climatic wind data to project wave climate under future warmer conditions. SWAN is a third generation spectral wave model developed by Delft University of Technology. The model has been extensively applied for wave simulation and hindcasting purposes in different locations (Akpınar et al., 2016; Kutupoğlu et al., 2018; Lin et al., 2002). Detailed descriptions of the model structure, mathematical formulations and applications have been presented in (Booij et al., 1999) and its manuals (e.g., SWAN user manual, 2018). It has a suitable performance for small scale, high-resolution applications due to considering generation, dissipation, and nonlinear wave-wave interactions. The basic equation applied in the model is the action balance equation that for a Cartesian coordinate can be formulated as (Ris et al., 1999):

$$\frac{\partial}{\partial t}N + \frac{\partial}{\partial x}C_x N + \frac{\partial}{\partial y}C_y N + \frac{\partial}{\partial \sigma}C_\sigma N + \frac{\partial}{\partial \theta}C_\theta N = \frac{S}{\sigma} \quad (10)$$

where N represents the action density, frequency (σ), wave direction (θ), spatial coordinate (x,y), time (t), and propagation velocity (C). The first three terms in the left hand side of equation 10 show temporal and spatial variation of N. The fourth term is representative of shifting effect of the relative frequency due to variations in depth and the fifth term denotes currents and the depth and current-induced refraction. *S* is source term which is a function of x,y,t,σ,θ reflecting effects of the generation by wind, dissipation (by white-capping, depth induced wave breaking and bottom friction) and nonlinear wave-wave interactions (Ris et al., 1999).

For this study, the SWAN model was set in a spherical coordinate and non-stationary mode. The computational domain covers the Persian Gulf from 47°E to 58°E of longitude and 23°N to 31°N of latitude (Figure 1). The spatial and temporal resolutions of the computational grid were set as 0.1° and 30 minute. Prior to implementation of the wave model for the future scenarios, the model was calibrated with wave data recorded by two buoys (W and M1 in Figure 1) located in Bushehr and Asaluyeh. The buoys records of wave characteristics with 1 hr interval have been employed. The Asaluyeh Buoy with coordinate of 52.5°E and 27.4°N is a node of the computational grid. On the other hand, the results for the Bushehr Buoy (50.67°E and 28.78°N) were interpolated because it is not located exactly on a node of the computational grid. However, a preliminary analysis considering the model resolution revealed that the error in wave height associated with this interpolation is less than 5%. As the buoys were located in deep water, the whitecapping dissipation coefficient (C_{ds}) using Komen et al. (1984) formulation was considered as tunable variable for the model calibration. Moreover, the quadruplet interaction was activated

using the model default formulation of Hasselmann et al. (1985). ERA5 wave data for 20 years and over the whole study area were also employed to conduct a multi-decadal validation. The ERA5 wave data (significant wave height of combined wind waves and swell) which was released recently have the spatial and temporal resolutions of 0.5×0.5 degrees and 1 hour, respectively. ERA5 is the last update of ECMWF reanalysis data combining a wide variety of historical observations into global estimates by means of data assimilation and numerical modelling. It should be noted that comparing the ERA5 wave data with those of the buoy measurements during 2008 indicated that ERA5 provides slightly higher wave heights than the buoy records. Regarding the outputs of the wave model during calibration and validation periods, the optimal value for C_{ds} was recognized as 3.25e-5. The other calibrated parameters were set as the model default. Results of the wave model for calibration and validation periods are given in Table 3.

Table 3. Results of the wave model for calibration and validation periods

	Buoy	Period	Bias (m)	R^2	RMSE (m)	MAE (m)
Calibration	Busherh	21/3/2008-7/9/2008	0.02	0.55	0.24	0.16
	Asaluyeh	21/3/2008-7/9/2008	-0.03	0.61	0.25	0.18
Validation	Busherh	1/2/1995-31/12/1995	-0.08	0.65	0.23	0.15
	Asaluyeh	14/2/2007-31/12/2008	0.03	0.39	0.28	0.20
	Whole domain (ERA5)	01/01/1981-31/12/2000	-0.17	0.67	0.18	0.17

The results presented in Table 3 show a relatively similar performance for both periods and Buoys. The error measures computed for the whole domain based on ERA5 wave data imply robustness of the model. These values have been averaged over the computational domain which indicate efficiency of the wave model in general. However, it should be noticed that the wave model underestimate peak values of significant wave heights. A thorough review on missing peaks in the current wave models have been addressed in Cavaleri (2009).

Prior to project wave climate for future scenarios, performance of the different GCMs and RCMs (MENA) wind outputs to simulate significant wave height in validation period was evaluated to select the appropriate model. In this regard, wind outputs of two GCMs (CMCC-CM and MPI-ESM-LR as well as CORDEX outputs of three models from MENA have been used to force wave model during 1991-2000. It is noticed that the GCM outputs have been modified based on the proposed downscaling method and the predictor-predictand relationships in calibration period (1981-1990). The results of wave models for different forcing resources during validation period (1991-2000) are presented in Table 4. The results are given in terms of average (Avg), standard deviation (Std), mean error (ME), and mean absolute error (MAE) of the significant wave height.

Table 4. Results of the wave model obtained using different GCMs/RCMs

GCM/RCM	Avg	Std	ME	MAE
ECMWF	36.84	30.86	-	-
CMCC	34.73	33.04	-2.11	2.15
MPI	27.59	28.13	-9.25	9.59
ECEARTH	27.00	27.71	-9.84	9.86
GFDL	30.36	33.47	-6.48	6.59
CNRM	27.59	28.58	-9.25	9.96

Table 4 demonstrates a high level of uncertainty associated with GCM/RCM selection for wave simulation. However, the CORDEX outputs of different RCMs projects roughly similar statistics for wave height except the GFDL model which outperforms the other two RCMs. Results of the wave model forcing with different wind resources can change reliability of the projection remarkably. However, it can be found that the wave model forced with wind outputs of CMCC-CM model yields the best consistency with those of the reference model in terms of error measures. Moreover, it is obtained that all the five models underestimate significant wave height compared to the results of the reference model. Considering different evaluation criteria for GCM/RCM selection in Table 3, the CMCC-CM wind outputs are used for wave projection under future scenarios.

3. Results and discussion

3.1. Wind modification

The proposed model was used to modify GCM wind data for two future projections RCP4.5 and RCP8.5 at each grid point, separately. Similarly, the QM technique as a common type statistical downscaling approach was employed to provide the comparison with the Weibull-based distributed model. In this regard, GCM historical data from 1981 to 2000 were divided into two groups of 10-years data of calibration (1981-1990) and validation (1991-2000) with stationary assumption for climate variation within these two periods. However, the preliminary investigation of statistical analysis for these periods revealed that the average (6 hourly averages for 10 years) and distribution of wind speed for these two periods roughly overlap each other. The results of downscaling techniques during validation period are compared with those of the reference data. The results in terms of average wind speed at four longitudes (transects 1 to 4) and throughout the whole latitude are presented in Figure 3. The transects 1 to 4 have longitudes of 49.5°E, 51.75°E, 54°E, and 56.25°E, respectively. Furthermore, two error measures of coefficient of determination (R^2) and root mean square error (RMSE) were applied to evaluate and also to provide more comparisons of performance of the techniques. The results during validation period for these 4 transects are presented in Table 5.

Figure 3. Wind speed variation alongside the latitude obtained from ECMWF, QM, and Weibull

Table 5. Results of the downscaling techniques in 4 transects during validation periods

Transect No.	QM		Weibull	
	R^2	RMSE (m/s)	R^2	RMSE (m/s)
1	0.89	0.22	0.99	0.14
2	0.91	0.29	0.99	0.18
3	0.78	0.45	0.98	0.19
4	0.60	0.40	0.93	0.16

According to Figure 3, the proposed model (Weibull-based) provides reasonable predictions of the wind speed for all the grid points. The predictions representing average wind speed during the validation period roughly overlapped the corresponding values of the reference data (ECMWF). Generally, the Weibull-based distributed model outperforms the QM technique even though their results are comparable for many grid points. The results presented in Table 5 indicate that the Weibull distribution based model outperforms the QM techniques in terms of R^2 and RMSE. A detailed comparison demonstrating superiority of the Weibull-based model over QM and also other statistical techniques for downscaling climatic wind field can be found in Alizadeh et al. (2019). Therefore, the proposed model can be efficiently applied for wind speed downscaling under future scenarios. It is noteworthy that the proposed statistical downscaling technique can be served as a suitable proxy to modify wind field, although the problem associated with effect of finer resolution that could reveal stronger extremes still remains unresolved. Figure 4 illustrates the average spatial distribution of the wind speed and also spatial variation of wind speed compared to historical data (100-year ago) for RCP4.5 in the left and for RCP8.5 in the right. Wind speeds depicted in Figure 4 have been obtained from the developed downscaling model, but not the raw outputs of the GCM.

Figure 4. Spatial variation of wind speed under future scenarios a) RCP4.5 b) RCP8.5; and the difference between past and future wind speeds c) RCP4.5 d) RCP8.5

As can be derived from Figure 4, wind speeds will be higher in the middle part of the Persian Gulf. The highest average rarely exceeds 6 m/s and its distribution does not follow any specific pattern. In some cases, remarkable spatial variation in wind speed can be observed especially in the middle and northwestern region of the Gulf. Moreover, the rate of variations differs from place to place which may reflect topographical effects or other spatial phenomena influencing wind speeds. As a result, the proposed model which modifies wind

data for each grid point is superior to the traditional inverse distance weighting method that may provide inaccurate or unreliable estimates for grid points with high gradient (high degree of variation) in the speed. Comparing the average values of wind speed for future projections demonstrates that the RCP4.5 projects slightly higher values than the RCP8.5. Generally, the spatial variation of wind speed in the study area implies a decreasing trend for most of the grid points (negative values). This decreasing rate is more remarkable in the western and middle part of the Persian Gulf. However, there are sporadic grid points in which, the wind speed experiences an increasing trend in the eastern part (positive values). Wind speed averages are in a range of 1.9 to 5 m/s while the relative variations are less than 16%. Considering the average wind speed in the whole grid points of RCP4.5 as 3.5 m/s, the variable is expected to experience an average rate of changes about 10-12%. Moreover, the results show that this variation rarely exceeds 16% for any grid points. It is notable that the average changes in wind speed are intensified when the RCP8.5 is replaced with the RCP4.5 projection. Therefore, considering the RCP8.5, the wind speed is expected to decrease at a higher rate in the future (2081-2100).

3.2. Wave modeling results

3.2.1. Annual variation of wave data

To investigate the impact of future climate change, wave in the area were simulated using wind data obtained from the proposed distributed model. The surface wind outputs of the GCM for two different scenarios have been taken under consideration and separate numerical model forcing with historical data were conducted. Comparison of the results of the wave models using historical and future wind projections demonstrates the climate change impacts in detail. The results of the mean significant wave height (H_s) for the study area and for historical (1981-2000) and also for future scenarios (2081-2100) are illustrated in Figure 5. These results are the 6hr wave model outputs averaged for 20-year period.

Figure 5. Results of the wave model for the historical and future H_s projection

Spatial distribution of H_s depicted in Figure 5 reveals that in the middle part of the Gulf higher averages of significant wave height are expected than other regions of the domain. Moreover, the lowest averages are obtained for the eastern part. Considering the bathymetry and spatial distribution of wind speed in the Persian Gulf, the middle part has longer fetch length and also higher values of wind speed. Therefore, higher averages of significant wave heights in the middle part of the Gulf are in line with wind variation and fetch length. Effect of wave fetch on future wave projections is expected to attenuate because of decreasing in average wind speed. However, it can not be analyzed properly without evaluation of future changes in bathymetry of the study area. Comparing the results of the wave model for historical (1981-2000) with those of

the future scenarios (2081-2100) reveals a decreasing trend in wave height. Rate of changes in significant wave height for RCP8.5 scenario is higher than the RCP4.5 scenario. Therefore, lower values in H_s averages for RCP8.5 is projected in the entire study area. A similar analysis for peak wave period (T_p) was carried out and the results are illustrated in Figure 6.

Figure 6. Results of the wave model for the historical and future T_p projection

In Figure 6, longer wave periods are projected for the middle section of the Gulf rather than the other regions due to having different fetch length, bathymetry and topography of the area. These results are in agreement with those of wave height projection and higher waves are obtained for the middle section. Future projections of the wave period in the study area reveal a decreasing trend roughly in the whole domain. This decrease in wave period is smaller for RCP4.5 scenario than the other scenario.

In addition to the results of the models over the entire computational domain, 4 stations locating in different parts of the study area from western part (*W*) to the middle part (*M1* and *M2*) and eastern part (*E*) of the Gulf with different depths (from 29 to 85m) are selected to provide quantitative and detailed descriptions. These points were selected based on their different wind and wave climate, as discussed by Kamranzad (2018). The station 1 (*W*) and 2 (*M1*) are near the Bushehr and Asaluyeh ports which are among the most important and strategic regions in the country. The station 3 (*E*) and 4 (*M2*) are located in the eastern and middle parts of the Gulf, respectively. The two other stations were selected to illustrate wave characteristic variations in the middle and eastern parts of the Gulf. The results of the wave models for significant wave height (average 'Avg.', 95% and 99% percentiles) are presented in Table 6.

Table 6. Results of significant wave height for different scenarios

Station no.	Historical			RCP4.5			RCP8.5		
(ID)	Avg.	$H_{95\%}$	$H_{99\%}$	Avg.	$H_{95\%}$	$H_{99\%}$	Avg.	$H_{95\%}$	$H_{99\%}$
1 (*W*)	0.32	0.82	1.16	0.29	0.72	1.04	0.28	0.70	1.02
2 (*M1*)	0.35	0.86	1.21	0.31	0.79	1.08	0.29	0.76	1.08
3 (*E*)	0.26	0.71	1.17	0.24	0.63	1.03	0.22	0.56	0.98
4 (*M2*)	0.47	1.45	2.19	0.42	1.31	1.93	0.39	1.19	1.85

The average values in Table 6 indicate that significant wave height for both scenarios experience a decrease compared with the corresponding values in the historical period. Generally, it can be concluded that the significant wave height in average decreases about 10% and 15% considering RCP4.5 and RCP8.5 future scenarios, respectively. Therefore, regardless of the projection scenarios, the wave climate in the future period of 2081 to 2100 has lower averages in the Persian Gulf compared to the historical values. The results are in line with the findings of Morim

et al. (2018) representing a decrease of average H_s in the North Atlantic and Mediterranean Sea. Considering the upper percentiles of the data (hereafter called extreme values), even though smaller extreme waves than historical period ones are expected, in some cases the extreme wave height may exceed the historical one. The probability and cumulative distributions of annual H_s for the selected stations during historical and future periods are illustrated in Figure 7.

Figure 7. Probability and cumulative distributions of annual significant wave height (H_s)

The wave climate in the past shows higher values than the future scenarios in all stations. Also, a smaller peakedness in the PDF of significant wave height in the past period can be observed, while its distribution implies greater values. Similar results can be extracted by comparing their CDFs. For the past climate, the lower values of the cumulative distribution function for the same wave height as the future scenarios confirms higher H_s in the past than the future. The wave period is another wave characteristic that may change in the future. In this regard, the results related to the peak wave period for the historical and future scenarios are extracted from the numerical wave model. The annual averages in peak wave period for the selected stations are given in Table 7.

Table 7. Annual average of peak wave period for different scenarios

Station no. (ID)	Historical	RCP4.5	RCP8.5
1 (*W*)	3.3	3.1	3.0
2 (*M1*)	3.5	3.4	3.3
3 (*E*)	3.2	3.1	3.0
4 (*M2*)	3.8	3.7	3.6

In line with the H_s results, the results of peak wave period for historical and future scenarios show a decreasing trend in prospective wave period. Moreover, the wave periods for the RCP8.5 have slightly smaller values than those of the RCP4.5. However, the difference is negligible (less than 3%). Therefore, it is expected that the future peak period in the Persian Gulf decrease by 5% for both of the scenarios. This decrease can be mainly considered as a result of decreasing in H_s (the lower waves, the shorter periods). It means the wave period is expected to decrease in the Persian Gulf under future scenarios due to a decrease about 15% in significant wave height. Therefore, considering annual average of H_s and peak period, it can be concluded that the wave climate under future scenarios is expected to experience smaller waves and also with shorter periods. The decrease in wave period and height under future climate is due to decrease in wind speed which is considered as the main driving force of waves. To get more detail of the changes in the wave climate and its distribution, the results of the wave models in seasonal and monthly scales are discussed in the following subsections.

Wave direction is another important wave characteristic while has attracted less attention than wave height and period in the global projections of wave climate. On the other hand, directional wave changes can affect longshore sediment transport and subsequently coastal erosion and deposition processes (Harley et al., 2017). Also, wave direction is an important variable for many other coastal activities such as renewable energy (Morim et al., 2016) and harbor operability (Sierra et al., 2017). To project changes in wave direction in the Persian Gulf, mean wave direction of the 6 hourly model output during a 20-year period of 1981-2000 and 2081-2100 are illustrated in Figure 8.

Figure 8. Mean wave direction over the study area

According to Figure 8 it can be concluded that the wave direction in the study area does not change significantly. Moreover, these changes do not follow any special pattern or trend. Regarding the wave direction near the eastern boundary it should be noted that the wave from Oman Seas influence the areas while their impacts were not considered. Comparing the mean wave direction derived from RCP4.5 and RCP8.5 demonstrate a slightly anticlockwise change in wave direction for RCP8.5 scenario. However, the wave direction is strongly dependent on the wind direction and bathymetry. Trend in Figure 8 is roughly consistent with the dominant wind direction (blowing from northwest). Similar to significant wave height and wave period, the results related to change in wave direction for 4 selected stations are also depicted in figures 9 to 12. It should be noticed that these results are plotted for the whole data of wave climate and the results of the seasonal and intra-annual distribution are not presented here for the sake of brevity.

Figure 9. Wave rose in station 1 for a) past, b) RCP4.5, and c) RCP8.5 scenarios

Figure 10. Wave rose in station 2 for a) past, b) RCP4.5, and c) RCP8.5 scenarios

Figure 11. Wave rose in station 3 for a) past, b) RCP4.5, and c) RCP8.5 scenarios

Figure 12. Wave rose in station 4 for a) past, b) RCP4.5, and c) RCP8.5 scenarios

From figures 9 to 12, it can be concluded that the future change in wave direction is highly dependent on the location of the selected station. In other words, in some locations the direction has not changed remarkably, while for some other locations, mild changes in the wave direction (station 4) can be found. These changes are mainly illustrated in the middle part of the Persian

583 Gulf (station 4) while the changes in western and eastern parts of the Persian Gulf are negligible
584 (stations 1 and 3). Generally, the dominant wave direction in all the stations under future
585 scenarios experience is roughly the same as the historical one. Generally, the wave direction in
586 the Persian Gulf due to its semi enclosed shape, topography and characteristics may not be
587 comparable with those obtained from global wave climate projections. The change in future
588 wave direction should be considered in future studies of sediment transport, port layout, coastal
589 geomorphology, etc. Moreover, this change can affect operability of the available ports in the
590 study area and change the coastal morphology due to changing in sediment transport pattern.

591 To understand whether these changes are due to climate change impacts or they are resulted from
592 internal climate variability of the system, inter-annual variability analysis was implemented. To
593 do that, inter-annual average and standard deviation for historical and future periods were
594 estimated and compared to illustrate the magnitude of changes in significant wave height. Figure
595 13 presents the results of inter-annual variability analysis for two RCPs against historical period.

596 Figure 13. Differences between historical projection of wave height and mean annual wave
597 height of RCP4.5 (a), RCP8.5 (b), and inter-annual standard deviation for RCP4.5 (c), and
598 RCP8.5 (d)

599 As seen in Figure 13, differences in mean significant wave height of historical and future
600 simulations are mostly larger than the differences in inter-annual standard deviation in future and
601 historical periods. This implies that the projected variations in the wave climate (under future
602 climatic conditions) are mainly due to climate change. The middle part of the Persian Gulf is
603 expected to have higher rate of variation in mean annual wave height while for the inter-annual
604 standard deviation, the variation is not monotonic and shows large spatial variability.

605

606 ### 3.2.2. Seasonal variation of wave characteristics

607 The seasonal distribution and variation of wave climate can provide more details of the climate
608 change impacts and it is of great interest for practical applications (renewable energy, coastal
609 protection, sediment transport, etc.). In this regard, results of the wave projections in terms of
610 wave height and wave period are analyzed to illustrate seasonal distribution of wave climate in
611 the Persian Gulf. The results related to seasonal average and seasonal extreme wave heights
612 (upper percentiles) are presented in Table 8. It is noticeable that for seasonal investigation, the
613 results have been evaluated based on the meteorological calendar.
614
615
616
617
618
619

Table 8. Seasonal analysis of significant wave height for different scenarios

Season	Station no. (ID)	Historical			RCP4.5			RCP8.5		
		Avg.	$H_{95\%}$	$H_{99\%}$	Avg.	$H_{95\%}$	$H_{99\%}$	Avg.	$H_{95\%}$	$H_{99\%}$
Winter	1 (*W*)	0.34	0.81	1.09	0.33	0.75	1.00	0.29	0.69	0.93
	2 (*M1*)	0.36	0.89	1.19	0.34	0.84	1.09	0.29	0.76	1.08
	3 (*E*)	0.28	0.84	1.33	0.24	0.74	1.27	0.19	0.58	0.99
	4 (*M2*)	0.56	1.70	2.33	0.53	1.54	2.11	0.44	1.35	2.07
Spring	1 (*W*)	0.30	0.72	1.02	0.29	0.67	0.97	0.28	0.67	0.96
	2 (*M1*)	0.37	0.86	1.21	0.36	0.88	1.14	0.35	0.85	1.13
	3 (*E*)	0.33	0.89	1.35	0.30	0.81	1.19	0.29	0.77	1.33
	4 (*M2*)	0.52	1.50	2.10	0.51	1.51	2.01	0.49	1.45	1.98
Summer	1 (*W*)	0.39	1.00	1.29	0.33	0.84	1.12	0.32	0.80	1.14
	2 (*M1*)	0.38	0.97	1.32	0.31	0.72	1.03	0.30	0.75	1.13
	3 (*E*)	0.23	0.48	0.76	0.23	0.47	0.67	0.24	0.47	0.63
	4 (*M2*)	0.44	1.32	2.31	0.35	0.93	1.66	0.36	1.00	1.69
Autumn	1 (*W*)	0.26	0.68	1.02	0.23	0.60	0.98	0.21	0.61	0.89
	2 (*M1*)	0.26	0.67	0.99	0.23	0.61	0.97	0.22	0.57	0.87
	3 (*E*)	0.19	0.44	0.68	0.17	0.40	0.72	0.17	0.40	0.59
	4 (*M2*)	0.34	1.01	1.78	0.30	0.91	1.67	0.28	0.81	1.38

Generally, it can be observed that wave distribution is more intensified in the winter among the other seasons. On the other hands, the smallest wave heights are projected for the autumn season. Moreover, station 4 (*M2*) has the highest average values and extremes for all the season. The main reason is that this station has been located in the middle part of the Persian Gulf where affected by the dominant wind more than other stations. The spatial distribution of wind speed demonstrate higher speeds in the middle part blowing from the North West of the Gulf which reflect the Shamal wind events in the region (Thoppil and Hogan, 2010). The results presented in Table 8 demonstrate that the average wave height for the future scenarios decreases for all the seasons. For both of scenarios, the lowest changes in the significant wave height are obtained for the spring season, while the highest changes for RCP4.5 and RCP8.5 are derived for summer and winter seasons, respectively. Similar to the average values, the extreme wave heights for all the seasons show a generally decreasing trend, even though it slightly increases for the winter season. Figure 14 depicts boxplot of H_s for each season separately to provide more illustrations. In the horizontal axes of the figure, the first letters (*P*, *L* and *H*) represent the past climate, future lower scenario (RCP4.5) and future higher scenario (RCP8.5), respectively. The second letter denoted with numeric from 1 to 4 stands for the station number.

Figure 14. Boxplots of seasonal significant wave height

It can be observed from Figure 14 that the significant wave height is higher in winter and lower in autumn. Moreover, the highest waves (extreme values) are occurring in station 4 (*M2*) in the middle part of the Persian Gulf where the dominant wind and topographical phenomena have the most and the least effects, respectively. Moreover, considering the lower concentration scenario (RCP4.5) yields greater extreme waves in all stations and seasons compared to the higher concentration scenario (RCP8.5). The black lines stand for minimum and maximum wave heights and crosses illustrate outliers. Moreover, the bottom, middle and top edges of the boxes represent first quartile, median and third quartile. Alongside with the wave height, seasonal variation of peak wave period has been taken under consideration and the results representing seasonal average in peak period are given in Table 9.

Table 9. Seasonal average of the peak wave period for different scenarios

Season	Station no. (ID)	Historical	RCP4.5	RCP8.5
Winter	1 (*W*)	3.4	3.4	3.2
	2 (*M1*)	3.6	3.6	3.3
	3 (*E*)	3.4	3.0	2.9
	4 (*M2*)	4.0	3.9	3.7
Spring	1 (*W*)	3.1	3.0	3.0
	2 (*M1*)	3.4	3.3	3.3
	3 (*E*)	3.5	3.4	3.3
	4 (*M2*)	3.9	3.9	3.8
Summer	1 (*W*)	3.6	3.4	3.3
	2 (*M1*)	3.8	3.6	3.6
	3 (*E*)	3.1	3.0	3.1
	4 (*M2*)	4.1	3.8	3.8
Autumn	1 (*W*)	3.0	2.8	2.7
	2 (*M1*)	3.1	3.0	2.9
	3 (*E*)	2.8	2.7	2.7
	4 (*M2*)	3.4	3.2	3.2

Generally, it can be found that the peak wave period in future projections experiences a decreasing rate. Moreover, station 4 (*M2*) has longer peak periods comparing to the other stations in the Persian Gulf. This can reflect higher values of wind speed in the middle part compared with the other regions (Figure 4). Considering the future scenario of RCP4.5, the highest decrease was projected for summer season while for the other scenario it was during winter season as 15%. However, the lowest changes in wave period are related to spring season for both scenarios while for the H_s it was obtained for autumn. The seasonal changes in significant wave height and period indicate that the wave height is changing with a higher rate than the wave

period in which demonstrate the future warmer climate may affect the wave height more than the wave period. The result is reasonable because the significant wave has more sensitivity to wind speed (w) than wave period ($H_s \sim w^{3/2}, T_p \sim w^{1/3}$). Considering the extreme values of wave characteristics it is pointed out that higher extremes compared to those of the obtained values are expected to happen due to incapability of the present wave models to simulate peak waves during severe and extreme storms. The wave models are generally tuned to the bulk of the data and may fail in extreme conditions when the physics of the process can change remarkably (Cavaleri, 2009). Moreover, effect of finer resolution with stronger extremes neglected in the statistical downscaling technique may lead to missing wave peaks as the wave model is forced with the coarser wind field.

3.2.3. Intra-annual variation of wave characteristics

Monthly distribution of wave characteristics and its variation under future scenarios can provide useful information for different purposes such as design and operation of coastal protection structures, renewable energies, and transportation and marine industries. In this regard, results of the historical and future scenarios of the numerical wave models for each month were obtained separately. Figure 15 illustrates the monthly average H_s and peak wave period T_p for historical (past) and future scenarios (RCP4.5 and RCP8.5).

Figure 15. Monthly variation of H_s and T_p for a) station 1, b) station 2, c) station 3, d) station 4

The results of the significant wave height and peak period imply that for stations 1, and 2 which are located in the western and middle onshore parts of the Persian Gulf, the highest values are obtained for month 6 (June). For the eastern station (no. 3), the highest wave height and period are obtained for month 5 (May). For the offshore middle station (no. 4), the highest wave height is obtained for February while the highest period is still for the June. Considering the meteorological calendar, the results are consistent with the common wind climate in which it blows mainly in summer (months 6 to 9) and winter (months 12, 1 ,2). However, the eastern part of the Persian Gulf is not affected by Shamal Wind or the dominant wind has the least effect on the station 3 (E) amongst the other stations. Therefore, it is reasonable to have a slightly different pattern of wind and wave climate in this station compared to the others. The results of the historical wave models are in a good accordance with those of the Kamranzad (2018) in terms of wave height and period.

According to Figure 15, the significant wave height and peak period decrease in the future roughly in all months and stations. A good consistency in monthly variation of the future wave projections and the historical wave climate can be observed in which, the average H_s and T_p

values in the future for each month rarely exceed the corresponding values in the past period. The rate of changes in future wave characteristics compared to the historical ones is higher in December, and June. For the other months, the changes are not remarkable. Following the future projections, it is estimated that the monthly average wave height in the Persian Gulf rarely exceeds 0.65 m. Moreover, for the monthly average of peak period, it is expected to change between 2.5 to 4.5 (*s*) under both future scenarios.

Results of monthly variation in wave climate obtained from this study are in line with findings of (Hemer et al., 2013a), which predicted a decrease annual significant wave height with higher rate during boreal winter (months 1 to 3) for future projections. Moreover, the decrease in annual significant wave height under future scenarios in the study area is in a good agreement with the results of the previous studies on projected changes in global wave climate (Hemer et al., 2013a; Semedo et al., 2012). The mentioned studies estimated a decrease in wave climate for lower latitudes of the study area. Also, for the wave period, the results of this study are consistent with the previous studies implying a mild decreasing trend in the wave period over the study area.

4. Summary and conclusion

In this study, a distributed approach to localize the wind projections, obtained from the global circulation models, has been employed and implemented to investigate future climate change impacts on the wave distribution. The proposed Weibull based method in its distributed form has been employed for the first time in this study to investigate climate change impacts on wave characteristics. The wind components obtained from the GCM of CMCC-CM have been used for the wave climate studies due to its better performance than the other considered GCM or RCMs. The modified wind components were utilized as forcing of the numerical wave model (SWAN) to analyze the wave characteristics including significant wave height (H_s) and peak wave period (T_p) in annual, seasonal and monthly time scales. Moreover, the average changes in wave direction in the future period in comparison with the historical period have been taken into consideration.

The proposed model for wind speed modifications showed that it can efficiently provide reliable predictions of wind speed. The results obtained through the verification period at several different locations in the study area confirmed this claim. Considering outputs related to wind speed under both future scenarios (RCP4.5 and RCP8.5) explored in this research, a decreasing trend with an average decrease about 10 to 15% can be estimated for the Persian Gulf. The changes in wind speed are expected to be more intensified in the middle and western parts of the Persian Gulf. However, this decrease rarely exceeds 0.6 m/s (15%) when the average annual wind speed is considered.

Regarding the average annual, seasonal and monthly wave projections for the future scenarios, it was estimated for the Persian Gulf to experience a decrease in annual, seasonal and monthly

736 average H_s in which, the rate of variation is higher for the middle parts of the Persian Gulf.
737 Moreover, the average H_s is expected to have more variation in winter (December to February)
738 and summer (June to August) among the other seasons. Generally, a decrease by 10 and 15% in
739 average annual H_s was projected for RCP4.5 and RCP8.5, respectively. Moreover, it was found
740 that with decreasing in average H_s, the extreme wave are expected to have smaller values than
741 those of the historical period, even though in some locations it may exceed the reported values.
742 For the study area, historical wave climate illustrates the highest averages of H_s occur in winter
743 and summer and the lowest averages during the autumn. For the future scenarios, the wave
744 climate is projected with a similar pattern, in which the highest average of H_s in winter and
745 summer and the smallest average of H_s remain for autumn.

746 Future projections of wave period in terms of annual average yielded a decrease about 5%. In
747 general, waves with shorter periods for the future years (2081-2100) and for all the seasons and
748 months were obtained comparing to the corresponding values in the historical period (1981-
749 2000). The average in peak wave period was found to have the highest values (longest period)
750 during June which is in line with highest average in H_s in the month.

751 The analysis of wave direction in the Persian Gulf demonstrated that in the western and eastern
752 locations, the future changes are insignificant. However, in the middle parts of the Persian Gulf,
753 a slightly clockwise rotation in wave direction was projected which is mainly affected by
754 changes in wind direction. However, effect of future changes in water depth and bathymetry may
755 change wave direction which was not considered in this study. This change can affect future
756 design and operation of marine industries, sediment transport processes and many other coastal
757 engineering applications. Regarding the two climatic future scenarios, the higher concentration
758 scenario (RCP8.5) intensifies changes in wave direction compared with the lower concentration
759 scenario (RCP4.5).

760 Comparison of future scenarios implies that the RCP4.5 has slightly projected higher values of
761 wind speed and significant wave height and also longer peak period than the RCP8.5. Moreover,
762 the RCP8.5 projected greater changes compared to the historical wind and wave climate rather
763 than the RCP4.5. Similar result was obtained for peak wave period. In brief, it can be concluded
764 that the future wave climate has somehow higher H_s and longer T_p in the lower concentration
765 scenario compared with the higher concentration scenario.

766 **Appendix A.**

767 The *MATLAB* code developed for downscaling wind field can be found via the following link.

768

769 **References**

770 Aarnes, O.J., Reistad, M., Breivik, Ø., Bitner-Gregersen, E., Ingolf Eide, L., Gramstad, O., Magnusson, A.K.,
771 Natvig, B., Vanem, E., 2017. Projected changes in significant wave height toward the end of the 21st
772 century: Northeast A tlantic. Journal of Geophysical Research: Oceans 122, 3394-3403.
773 Abbasian, M., Moghim, S., Abrishamchi, A., 2019. Performance of the general circulation models in
774 simulating temperature and precipitation over Iran. Theoretical and Applied Climatology 135, 1465-
775 1483.
776 Akpınar, A., Bingölbali, B., Van Vledder, G.P., 2016. Wind and wave characteristics in the Black Sea based
777 on the SWAN wave model forced with the CFSR winds. Ocean Engineering 126, 276-298.
778 Alizadeh, M.J., Kavianpour, M.R., Kamranzad, B., Etemad-Shahidi, A., 2019. A Weibull Distribution Based
779 Technique for Downscaling of Climatic Wind Field. Asia-Pacific Journal of Atmospheric Sciences, 1-16.
780 Amirinia, G., Kamranzad, B., Mafi, S., 2017. Wind and wave energy potential in southern Caspian Sea
781 using uncertainty analysis. Energy 120, 332-345.
782 Bitner-Gregersen, E.M., Dong, S., Fu, T., Ma, N., Maisondieu, C., Miyake, R., Rychlik, I., 2016. Sea state
783 conditions for marine structures' analysis and model tests. Ocean Engineering 119, 309-322.
784 Booij, N., Ris, R., Holthuijsen, L.H., 1999. A third-generation wave model for coastal regions: 1. Model
785 description and validation. Journal of geophysical research: Oceans 104, 7649-7666.
786 Breslow, P.B., Sailor, D.J., 2002. Vulnerability of wind power resources to climate change in the
787 continental United States. Renewable Energy 27, 585-598.
788 Burrough, P.A., McDonnell, R.A., 1998. Creating continuous surfaces from point data. Principles of
789 Geographic Information Systems. Oxford University Press, Oxford, UK.
790 Caires, S., Swail, V.R., Wang, X.L., 2006. Projection and analysis of extreme wave climate. Journal of
791 Climate 19, 5581-5605.
792 Camus, P., Losada, I., Izaguirre, C., Espejo, A., Menéndez, M., Pérez, J., 2017. Statistical wave climate
793 projections for coastal impact assessments. Earth's Future 5, 918-933.
794 Casas-Prat, M., Wang, X., Swart, N., 2018. CMIP5-based global wave climate projections including the
795 entire Arctic Ocean. Ocean Modelling 123, 66-85.
796 Cavaleri, L., 2009. Wave modeling—Missing the peaks. Journal of Physical Oceanography 39, 2757-2778.
797 Chang, T.-J., Chen, C.-L., Tu, Y.-L., Yeh, H.-T., Wu, Y.-T., 2015. Evaluation of the climate change impact on
798 wind resources in Taiwan Strait. Energy Conversion and Management 95, 435-445.
799 Chang, T.-J., Wu, Y.-T., Hsu, H.-Y., Chu, C.-R., Liao, C.-M., 2003. Assessment of wind characteristics and
800 wind turbine characteristics in Taiwan. Renewable energy 28, 851-871.
801 Dee, D.P., Uppala, S.M., Simmons, A., Berrisford, P., Poli, P., Kobayashi, S., Andrae, U., Balmaseda, M.,
802 Balsamo, G., Bauer, d.P., 2011. The ERA-Interim reanalysis: Configuration and performance of the data
803 assimilation system. Quarterly Journal of the royal meteorological society 137, 553-597.
804 Dixon, K.W., Lanzante, J.R., Nath, M.J., Hayhoe, K., Stoner, A., Radhakrishnan, A., Balaji, V., Gaitán, C.F.,
805 2016. Evaluating the stationarity assumption in statistically downscaled climate projections: is past
806 performance an indicator of future results? Climatic Change 135, 395-408.
807 Goly, A., Teegavarapu, R.S., Mondal, A., 2014. Development and evaluation of statistical downscaling
808 models for monthly precipitation. Earth Interactions 18, 1-28.
809 Harley, M.D., Turner, I.L., Kinsela, M.A., Middleton, J.H., Mumford, P.J., Splinter, K.D., Phillips, M.S.,
810 Simmons, J.A., Hanslow, D.J., Short, A.D., 2017. Extreme coastal erosion enhanced by anomalous
811 extratropical storm wave direction. Scientific reports 7, 6033.
812 Hasselmann, S., Hasselmann, K., Allender, J., Barnett, T., 1985. Computations and parameterizations of
813 the nonlinear energy transfer in a gravity-wave specturm. Part II: Parameterizations of the nonlinear
814 energy transfer for application in wave models. Journal of Physical Oceanography 15, 1378-1391.
815 Hegermiller, C., Antolinez, J.A., Rueda, A., Camus, P., Perez, J., Erikson, L., Barnard, P., Mendez, F.J.,
816 2017. A multimodal wave spectrum–based approach for statistical downscaling of local wave climate.
817 Journal of Physical Oceanography 47, 375-386.

818 Hemer, M.A., Fan, Y., Mori, N., Semedo, A., Wang, X.L., 2013a. Projected changes in wave climate from a
819 multi-model ensemble. Nature climate change 3, 471.
820 Hemer, M.A., Katzfey, J., Trenham, C.E., 2013b. Global dynamical projections of surface ocean wave
821 climate for a future high greenhouse gas emission scenario. Ocean Modelling 70, 221-245.
822 Kamranzad, B., 2018. Persian Gulf zone classification based on the wind and wave climate variability.
823 Ocean Engineering 169, 604-635.
824 Kamranzad, B., Chegini, V., Etemad-Shahidi, A., 2016. Temporal-spatial variation of wave energy and
825 nearshore hotspots in the Gulf of Oman based on locally generated wind waves. Renewable Energy 94,
826 341-352.
827 Kamranzad, B., Etemad-Shahidi, A., Chegini, V., Yeganeh-Bakhtiary, A., 2015. Climate change impact on
828 wave energy in the Persian Gulf. Ocean Dynamics 65, 777-794.
829 Khan, N., Shahid, S., Ahmed, K., Ismail, T., Nawaz, N., Son, M., 2018. Performance assessment of general
830 circulation model in simulating daily precipitation and temperature using multiple gridded datasets.
831 Water 10, 1793.
832 Komen, G., Hasselmann, K., Hasselmann, K., 1984. On the existence of a fully developed wind-sea
833 spectrum. Journal of physical oceanography 14, 1271-1285.
834 Kutupoğlu, V., Çakmak, R.E., Akpınar, A., van Vledder, G.P., 2018. Setup and evaluation of a SWAN wind
835 wave model for the Sea of Marmara. Ocean Engineering 165, 450-464.
836 Lemos, G., Semedo, A., Dobrynin, M., Behrens, A., Staneva, J., Bidlot, J.-R., Miranda, P.M., 2019. Mid-
837 twenty-first century global wave climate projections: Results from a dynamic CMIP5 based ensemble.
838 Global and Planetary Change 172, 69-87.
839 Li, H., Sheffield, J., Wood, E.F., 2010. Bias correction of monthly precipitation and temperature fields
840 from Intergovernmental Panel on Climate Change AR4 models using equidistant quantile matching.
841 Journal of Geophysical Research: Atmospheres 115.
842 Lin, W., Sanford, L.P., Suttles, S.E., 2002. Wave measurement and modeling in Chesapeake Bay.
843 Continental Shelf Research 22, 2673-2686.
844 Mishra, V., Kumar, D., Ganguly, A.R., Sanjay, J., Mujumdar, M., Krishnan, R., Shah, R.D., 2014. Reliability
845 of regional and global climate models to simulate precipitation extremes over India. Journal of
846 Geophysical Research: Atmospheres 119, 9301-9323.
847 Morim, J., Cartwright, N., Etemad-Shahidi, A., Strauss, D., Hemer, M., 2016. Wave energy resource
848 assessment along the Southeast coast of Australia on the basis of a 31-year hindcast. Applied energy
849 184, 276-297.
850 Morim, J., Hemer, M., Cartwright, N., Strauss, D., Andutta, F., 2018. On the concordance of 21st century
851 wind-wave climate projections. Global and Planetary Change.
852 Patra, A., Bhaskaran, P.K., 2017. Temporal variability in wind–wave climate and its validation with ESSO-
853 NIOT wave atlas for the head Bay of Bengal. Climate Dynamics 49, 1271-1288.
854 Perez, J., Menendez, M., Mendez, F.J., Losada, I.J., 2014. Evaluating the performance of CMIP3 and
855 CMIP5 global climate models over the north-east Atlantic region. Climate dynamics 43, 2663-2680.
856 Ris, R., Holthuijsen, L., Booij, N., 1999. A third-generation wave model for coastal regions: 2. Verification.
857 Journal of Geophysical Research: Oceans 104, 7667-7681.
858 Ruest, B., Neumeier, U., Dumont, D., Bismuth, E., Senneville, S., Caveen, J., 2016. Recent wave climate
859 and expected future changes in the seasonally ice-infested waters of the Gulf of St. Lawrence, Canada.
860 Climate dynamics 46, 449-466.
861 Sangelantoni, L., Russo, A., Gennaretti, F., 2018. Impact of bias correction and downscaling through
862 quantile mapping on simulated climate change signal: a case study over Central Italy. Theoretical and
863 Applied Climatology, 1-16.
864 Semedo, A., Dobrynin, M., Lemos, G., Behrens, A., Staneva, J., de Vries, H., Sterl, A., Bidlot, J.-R.,
865 Miranda, P., Murawski, J., 2018. CMIP5-Derived Single-Forcing, Single-Model, and Single-Scenario Wind-

Wave Climate Ensemble: Configuration and Performance Evaluation. Journal of Marine Science and Engineering 6, 90.
Semedo, A., Sušelj, K., Rutgersson, A., Sterl, A., 2011. A global view on the wind sea and swell climate and variability from ERA-40. Journal of Climate 24, 1461-1479.
Semedo, A., Weisse, R., Behrens, A., Sterl, A., Bengtsson, L., Günther, H., 2012. Projection of global wave climate change toward the end of the twenty-first century. Journal of Climate 26, 8269-8288.
Shin, J.-Y., Jeong, C., Heo, J.-H., 2018. A Novel Statistical Method to Temporally Downscale Wind Speed Weibull Distribution Using Scaling Property. Energies 11, 633.
Shirkhani, H., Seidou, O., Mohammadian, A., Qiblawey, H., 2015. Projection of significant wave height in a coastal area under RCPs climate change scenarios. Natural Hazards Review 17, 04015016.
Sierra, J., Genius, A., Lionello, P., Mestres, M., Mösso, C., Marzo, L., 2017. Modelling the impact of climate change on harbour operability: The Barcelona port case study. Ocean Engineering 141, 64-78.
Themeßl, M.J., Gobiet, A., Heinrich, G., 2012. Empirical-statistical downscaling and error correction of regional climate models and its impact on the climate change signal. Climatic Change 112, 449-468.
Thoppil, P.G., Hogan, P.J., 2010. Persian Gulf response to a wintertime shamal wind event. Deep Sea Research Part I: Oceanographic Research Papers 57, 946-955.
Tye, M.R., Stephenson, D.B., Holland, G.J., Katz, R.W., 2014. A Weibull approach for improving climate model projections of tropical cyclone wind-speed distributions. Journal of Climate 27, 6119-6133.
Vanem, E., 2015. Non-stationary extreme value models to account for trends and shifts in the extreme wave climate due to climate change. Applied Ocean Research 52, 201-211.
Wandres, M., Pattiaratchi, C., Hemer, M.A., 2017. Projected changes of the southwest Australian wave climate under two atmospheric greenhouse gas concentration pathways. Ocean Modelling 117, 70-87.
Wandres, M., Pattiaratchi, C., Hetzel, Y., Wijeratne, E., 2018. The response of the southwest Western Australian wave climate to Indian Ocean climate variability. Climate Dynamics 50, 1533-1557.
Wang, L., Perrie, W., Long, Z., Blokhina, M., Zhang, G., Toulany, B., Zhang, M., 2018. The impact of climate change on the wave climate in the Gulf of St. Lawrence. Ocean Modelling 128, 87-101.
Wang, X.L., Feng, Y., Swail, V.R., 2014. Changes in global ocean wave heights as projected using multimodel CMIP5 simulations. Geophysical Research Letters 41, 1026-1034.
Wang, X.L., Feng, Y., Swail, V.R., 2015. Climate change signal and uncertainty in CMIP5-based projections of global ocean surface wave heights. Journal of Geophysical Research: Oceans 120, 3859-3871.
Wang, X.L., Swail, V.R., Cox, A., 2010. Dynamical versus statistical downscaling methods for ocean wave heights. International Journal of Climatology: A Journal of the Royal Meteorological Society 30, 317-332.

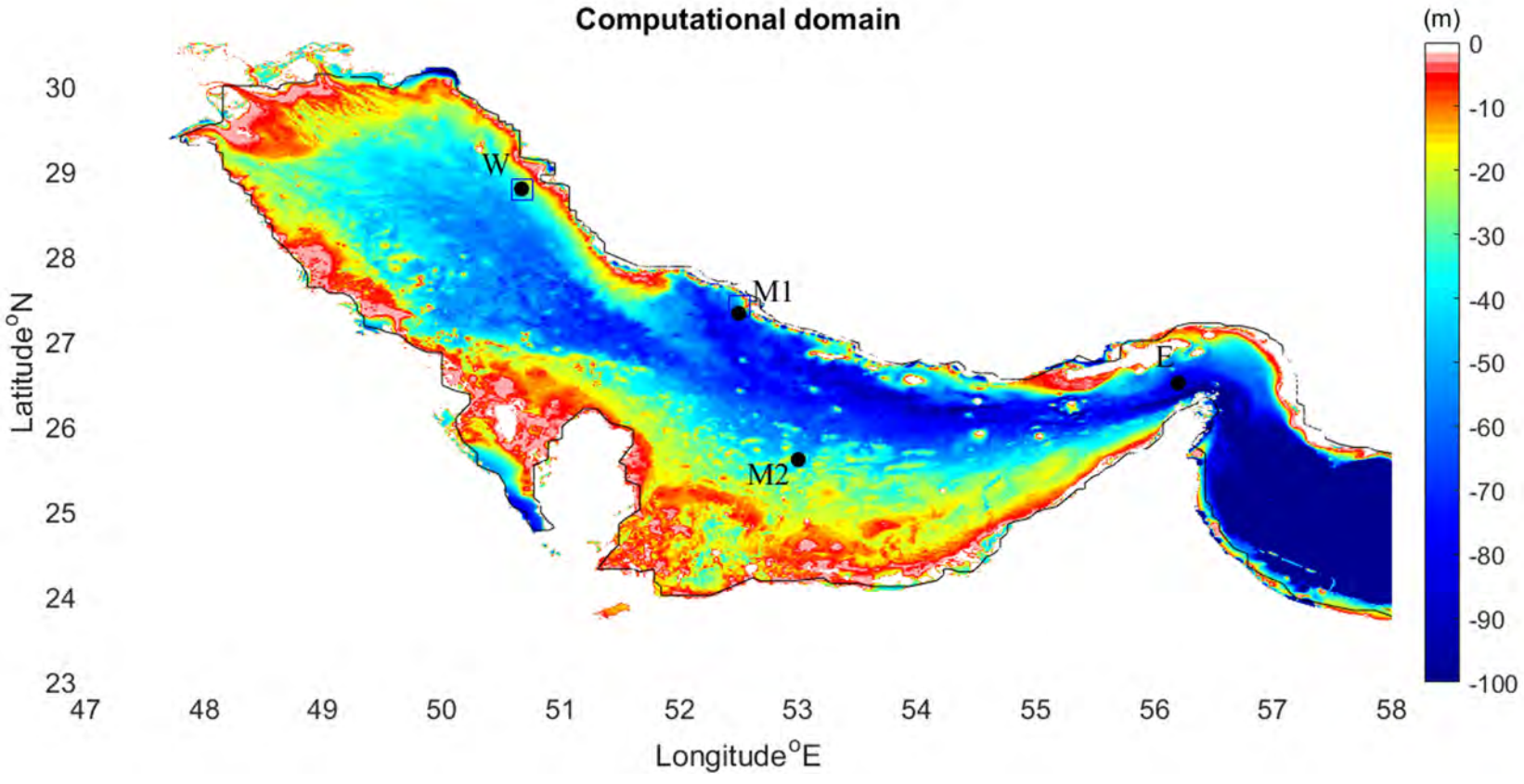
Computational domain
(m)
0
-10
-20
-30
-40
-50
-60
-70
-80
-90
-100
W
M1
M2
E
Latitude°N
Longitude°E
30
29
28
27
26
25
24
23
47
48
49
50
51
52
53
54
55
56
57
58

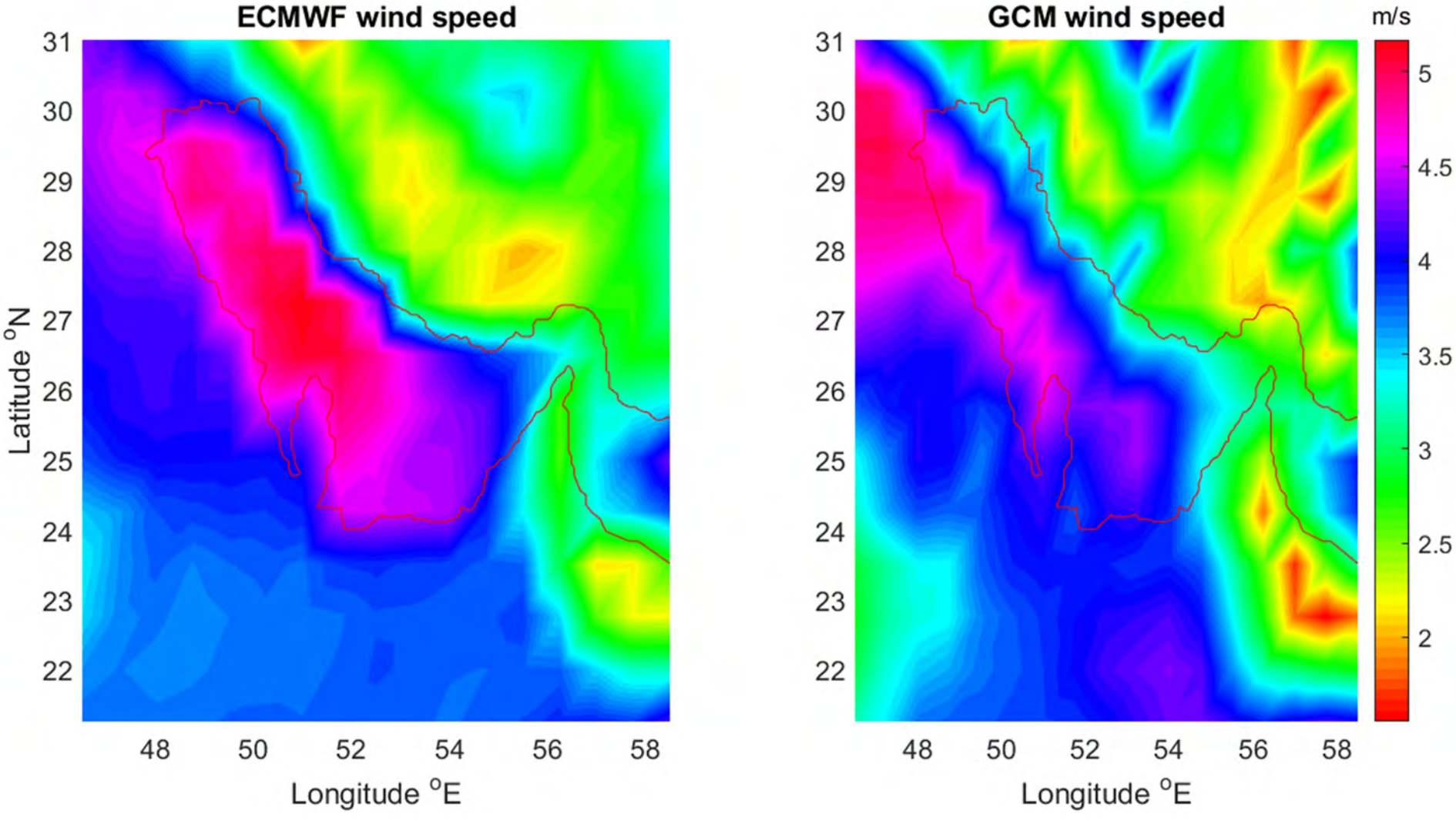
ECMWF wind speed
GCM wind speed
m/s
5
4.5
4
3.5
3
2.5
2
31
30
29
28
27
26
25
24
23
22
Latitude °N
48
50
52
54
56
58
Longitude °E

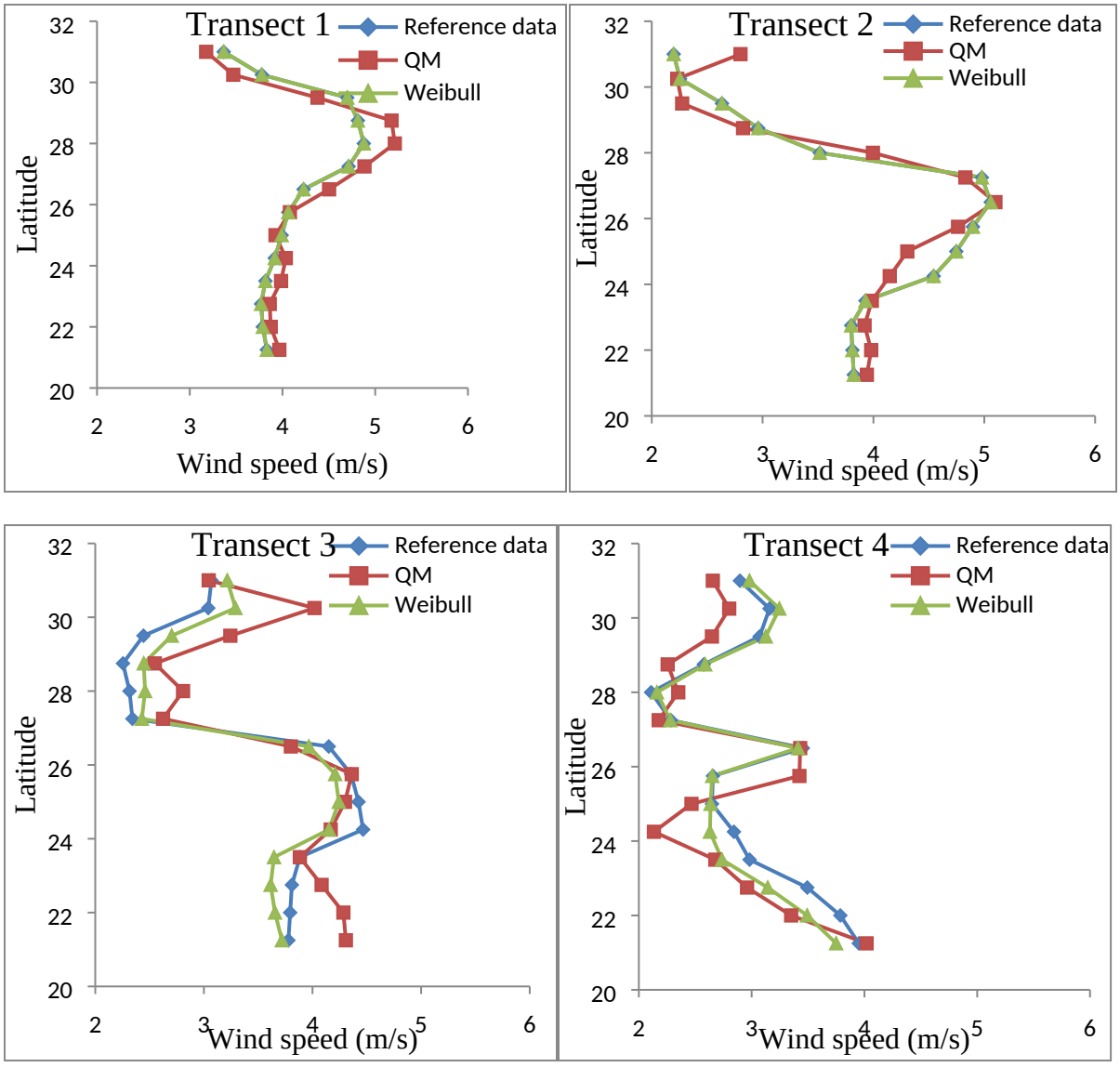
Transect 1
Reference data
QM
Weibull
Latitude
Wind speed (m/s)
Transect 2
Reference data
QM
Weibull
Latitude
Wind speed (m/s)
Transect 3
Reference data
QM
Weibull
Latitude
Wind speed (m/s)
Transect 4
Reference data
QM
Weibull
Latitude
Wind speed (m/s)

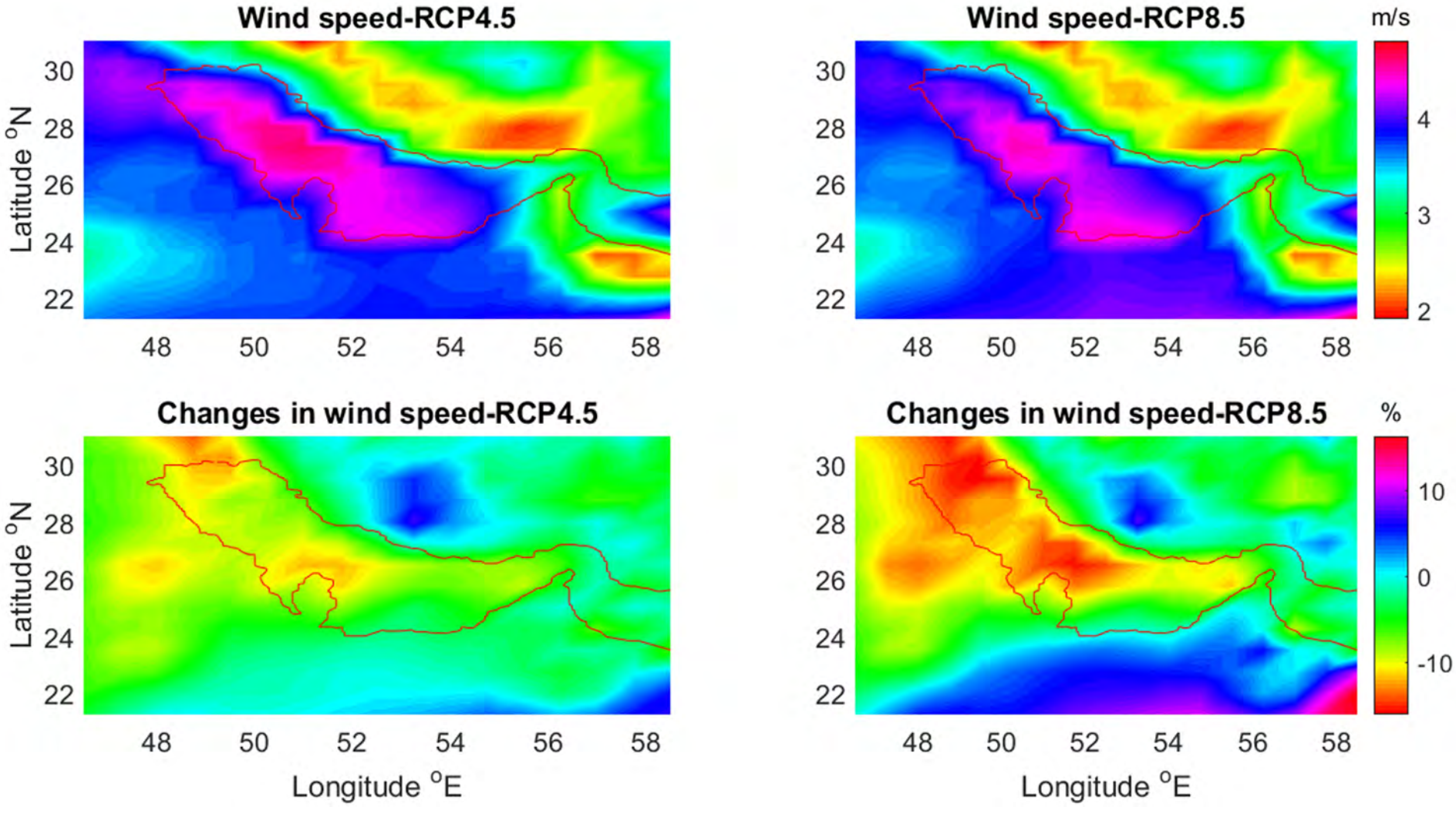
Wind speed-RCP4.5
Wind speed-RCP8.5
m/s
Changes in wind speed-RCP4.5
Changes in wind speed-RCP8.5
%
Latitude °N
Longitude °E
30
28
26
24
22
48
50
52
54
56
58
4
3
2
10
0
-10

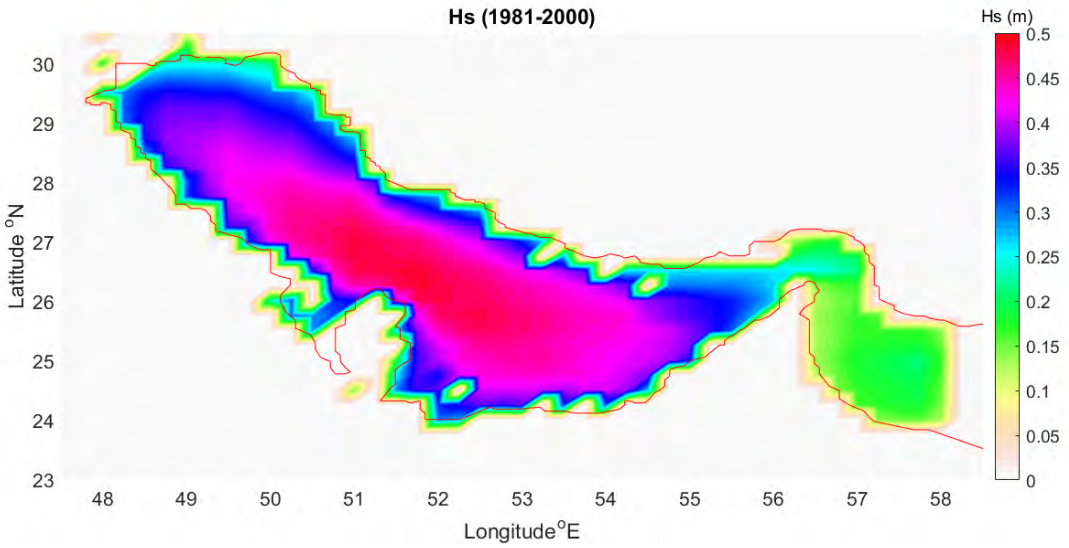
Hs (1981-2000)
Hs (m)
0.5
0.45
0.4
0.35
0.3
0.25
0.2
0.15
0.1
0.05
0
30
29
28
27
26
25
24
23
Latitude °N
48
49
50
51
52
53
54
55
56
57
58
Longitude °E

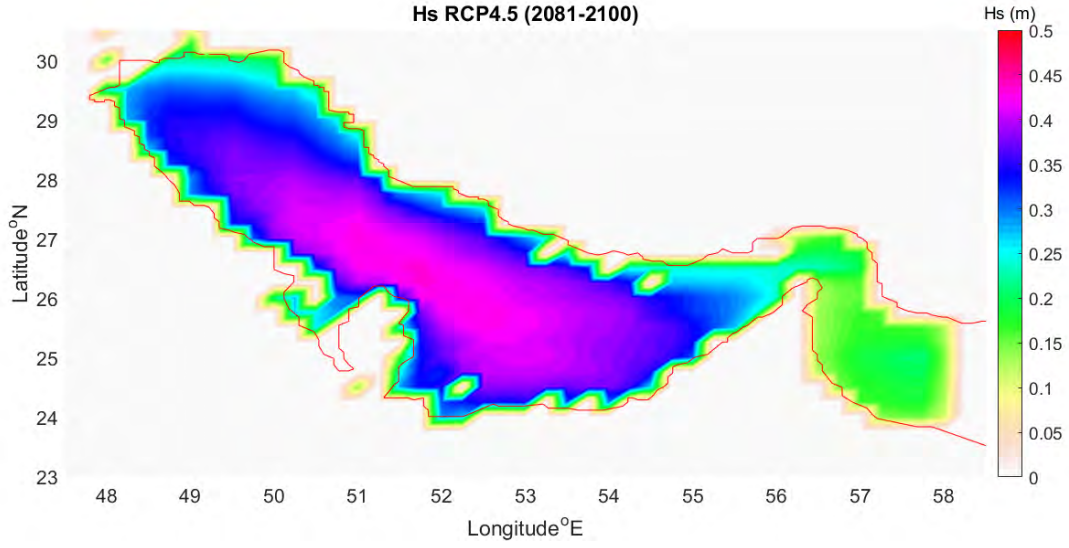
Hs RCP4.5 (2081-2100)
Hs (m)
0.5
0.45
0.4
0.35
0.3
0.25
0.2
0.15
0.1
0.05
0
30
29
28
27
26
25
24
23
Latitude °N
48
49
50
51
52
53
54
55
56
57
58
Longitude °E

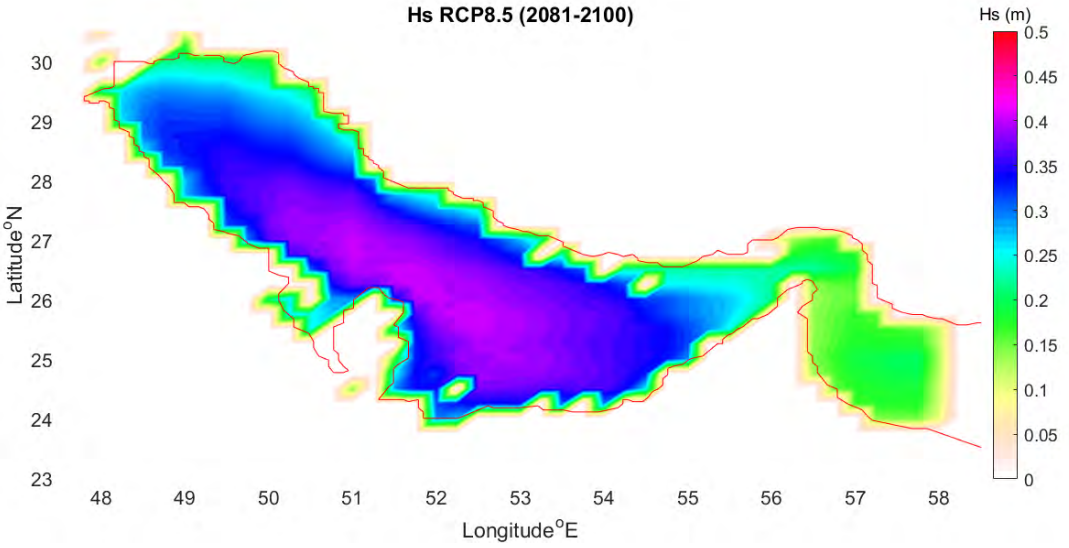
Hs RCP8.5 (2081-2100)
Hs (m)
0.5
0.45
0.4
0.35
0.3
0.25
0.2
0.15
0.1
0.05
0
30
29
28
27
26
25
24
23
Latitude °N
48
49
50
51
52
53
54
55
56
57
58
Longitude °E

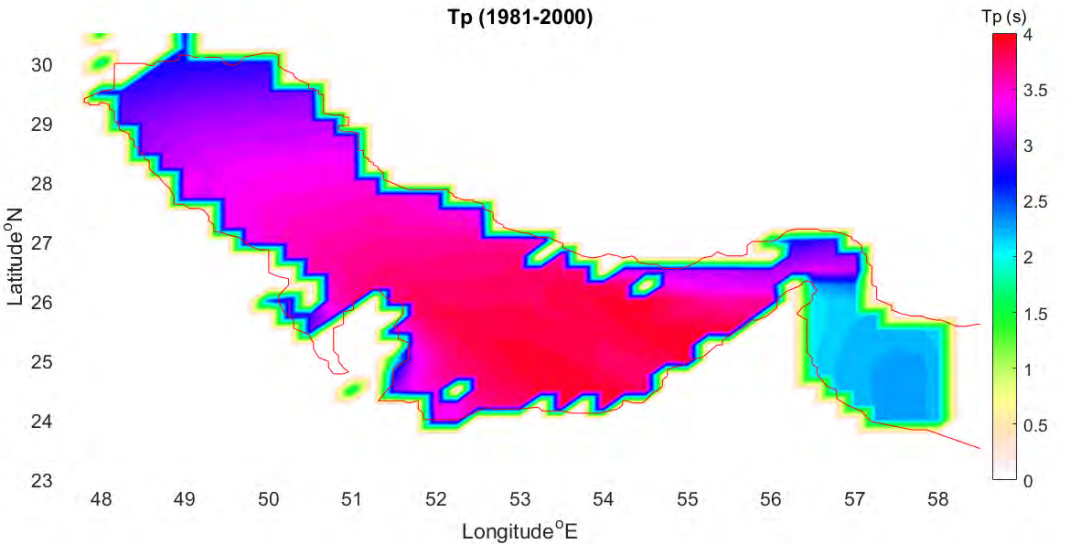
Tp (1981-2000)
Tp (s)
4
3.5
3
2.5
2
1.5
1
0.5
0
Latitude°N
30
29
28
27
26
25
24
23
48
49
50
51
52
53
54
55
56
57
58
Longitude°E

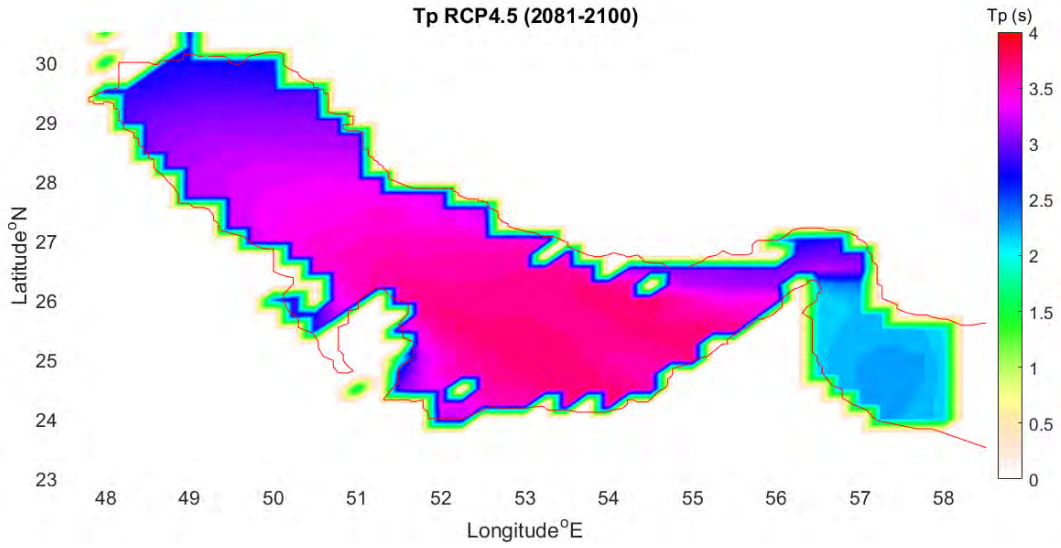
Tp RCP4.5 (2081-2100)
Tp (s)
4
3.5
3
2.5
2
1.5
1
0.5
0
Latitude°N
30
29
28
27
26
25
24
23
48
49
50
51
52
53
54
55
56
57
58
Longitude°E

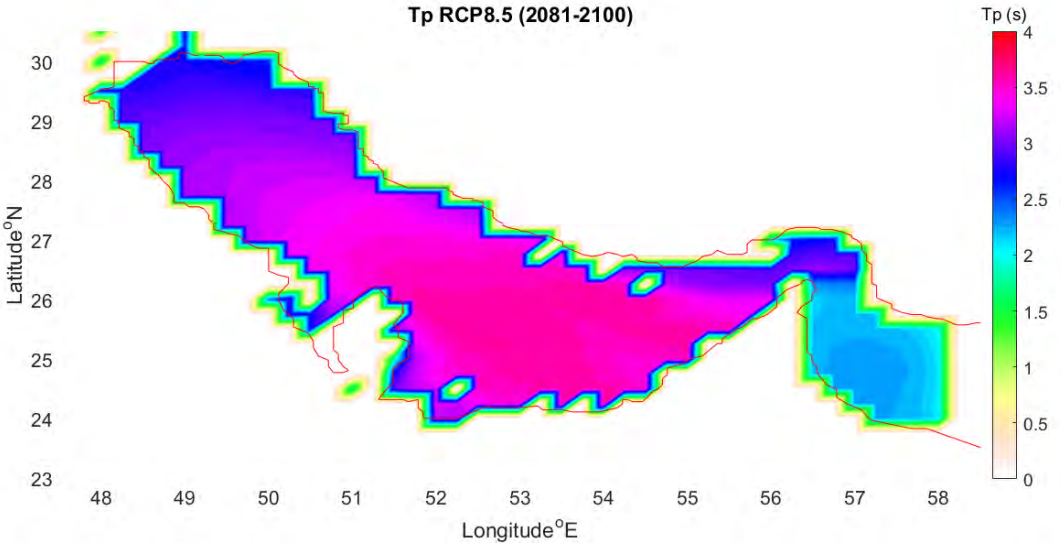
Tp RCP8.5 (2081-2100)
Tp (s)
4
3.5
3
2.5
2
1.5
1
0.5
0
Latitude°N
30
29
28
27
26
25
24
23
48
49
50
51
52
53
54
55
56
57
58
Longitude°E

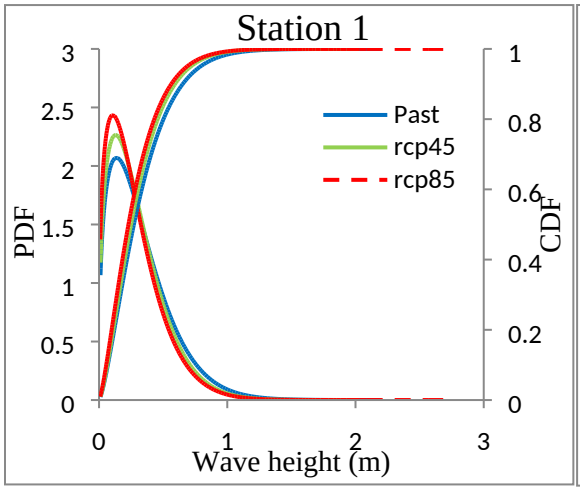
Station 1
PDF
CDF
Past
rcp45
rcp85
Wave height (m)

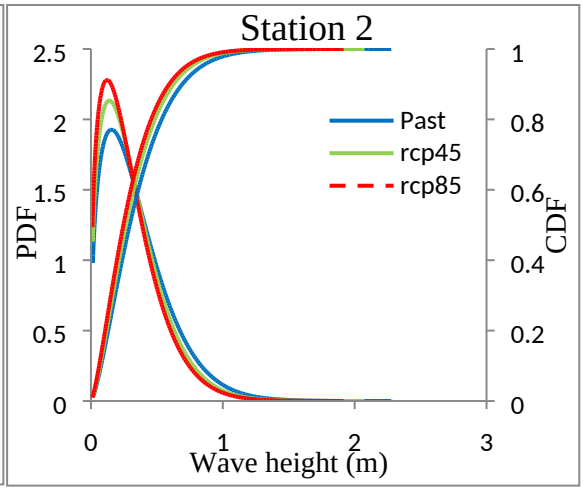
Station 2
PDF
CDF
Past
rcp45
rcp85
Wave height (m)

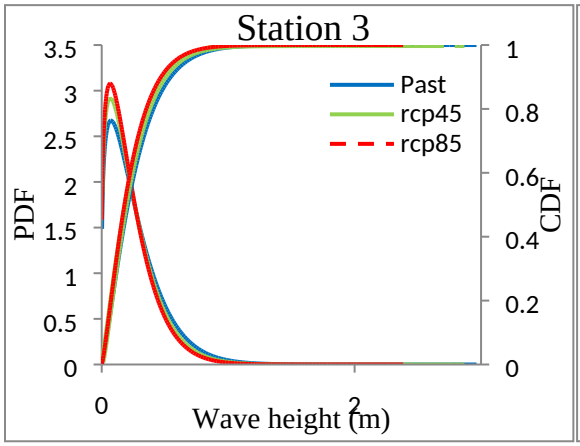
Station 3
PDF
CDF
Past
rcp45
rcp85
Wave height (m)

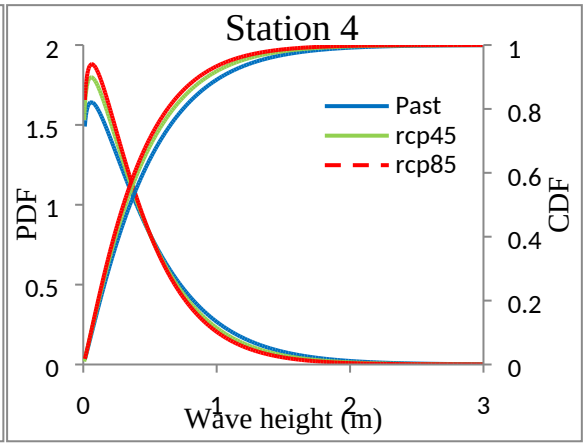
Station 4
PDF
CDF
Past
rcp45
rcp85
Wave height (m)

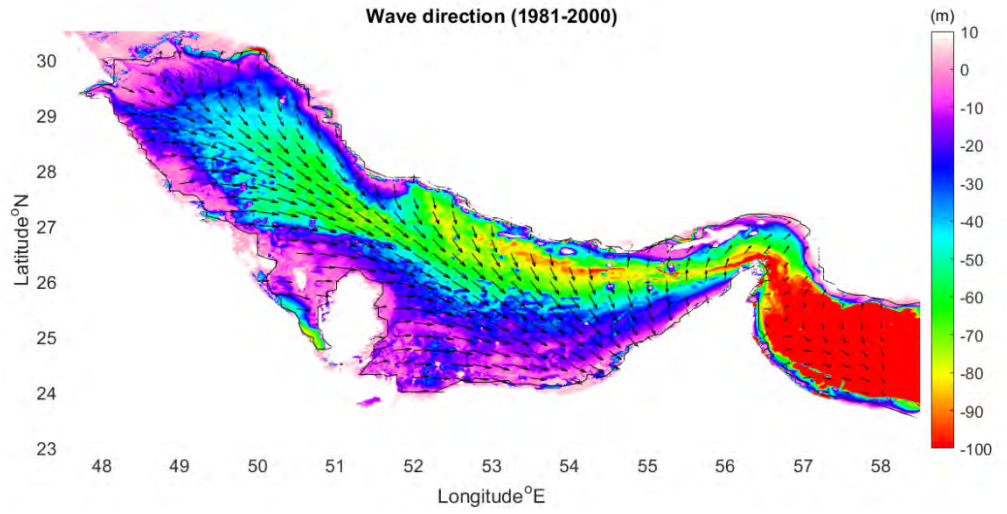
Wave direction (1981-2000)
(m)
10
0
-10
-20
-30
-40
-50
-60
-70
-80
-90
-100
30
29
28
27
26
25
24
23
Latitude°N
48
49
50
51
52
53
54
55
56
57
58
Longitude°E

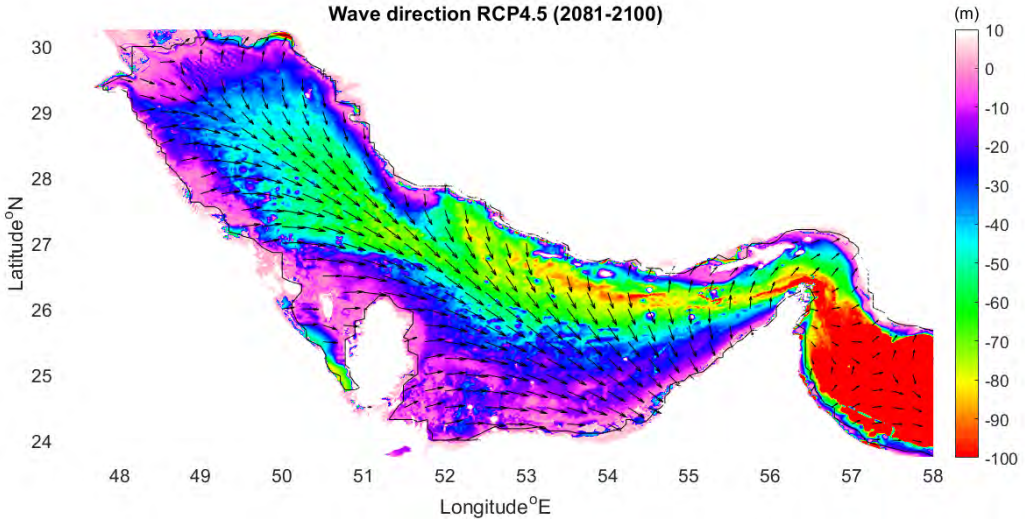
Wave direction RCP4.5 (2081-2100)
(m)
10
0
-10
-20
-30
-40
-50
-60
-70
-80
-90
-100
30
29
28
27
26
25
24
Latitude°N
48
49
50
51
52
53
54
55
56
57
58
Longitude°E

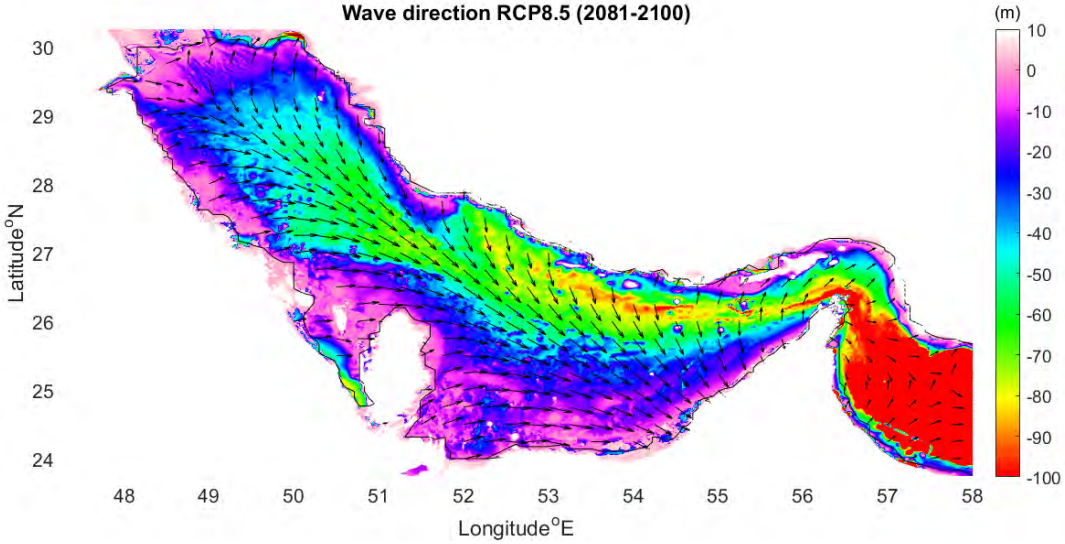
Wave direction RCP8.5 (2081-2100)
(m)
10
0
-10
-20
-30
-40
-50
-60
-70
-80
-90
-100
30
29
28
27
26
25
24
Latitude°N
48
49
50
51
52
53
54
55
56
57
58
Longitude°E

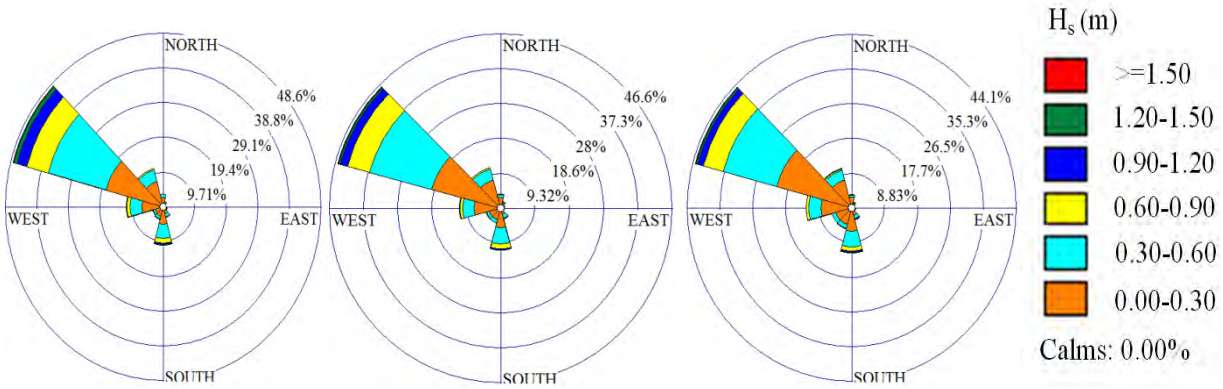

a) Past b) RCP4.5 c) RCP8.5

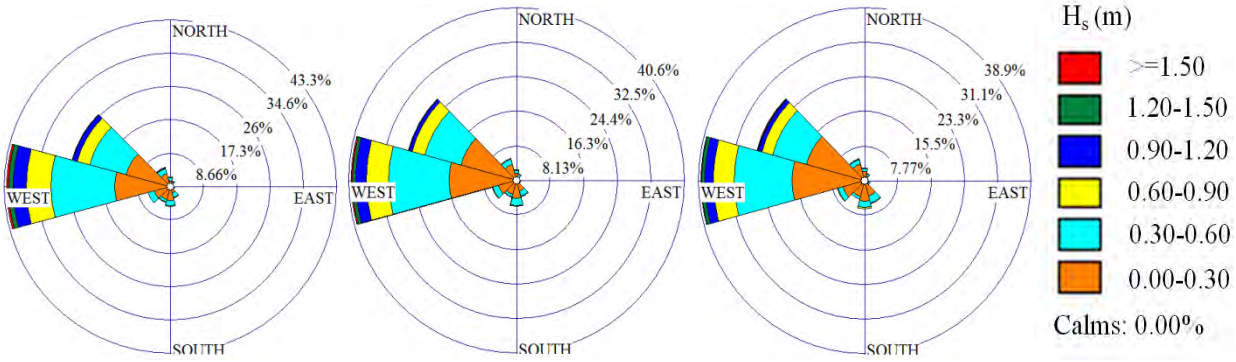

a) Past b) RCP4.5 c) RCP8.5

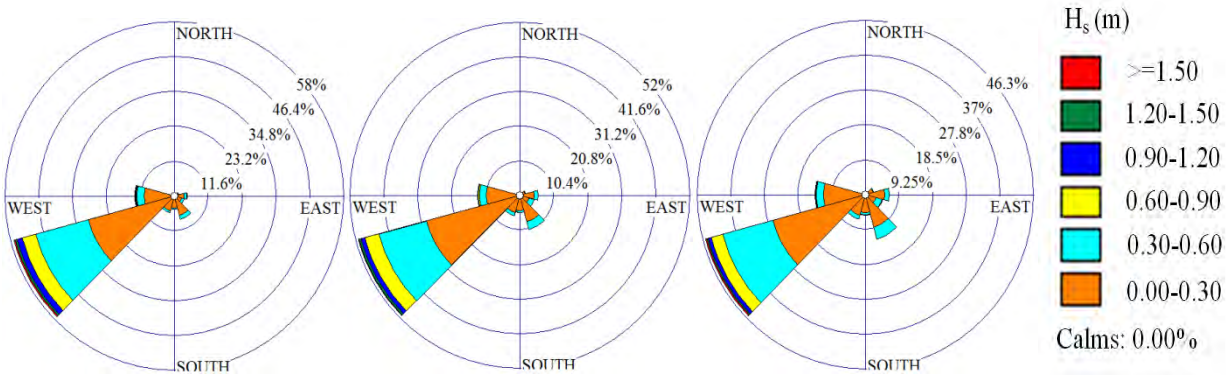

a) Past b) RCP4.5 c) RCP8.5

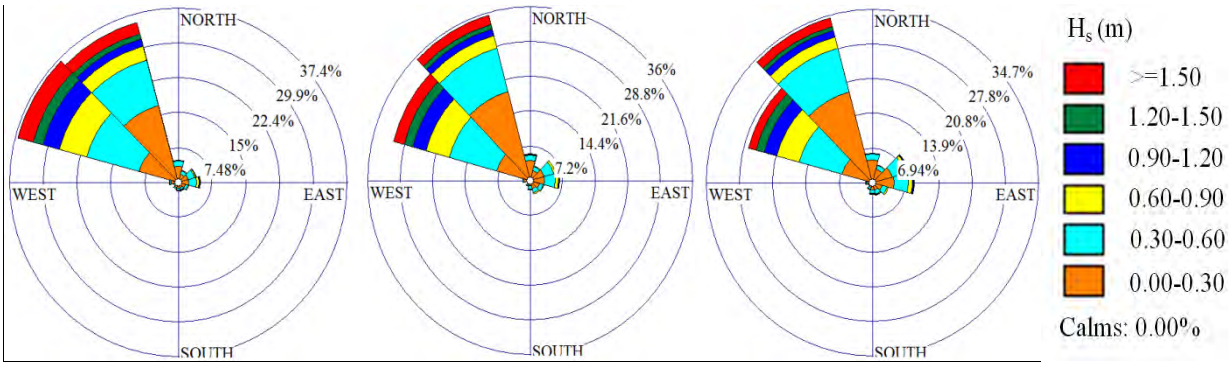

a) Past b) RCP4.5 c) RCP8.5

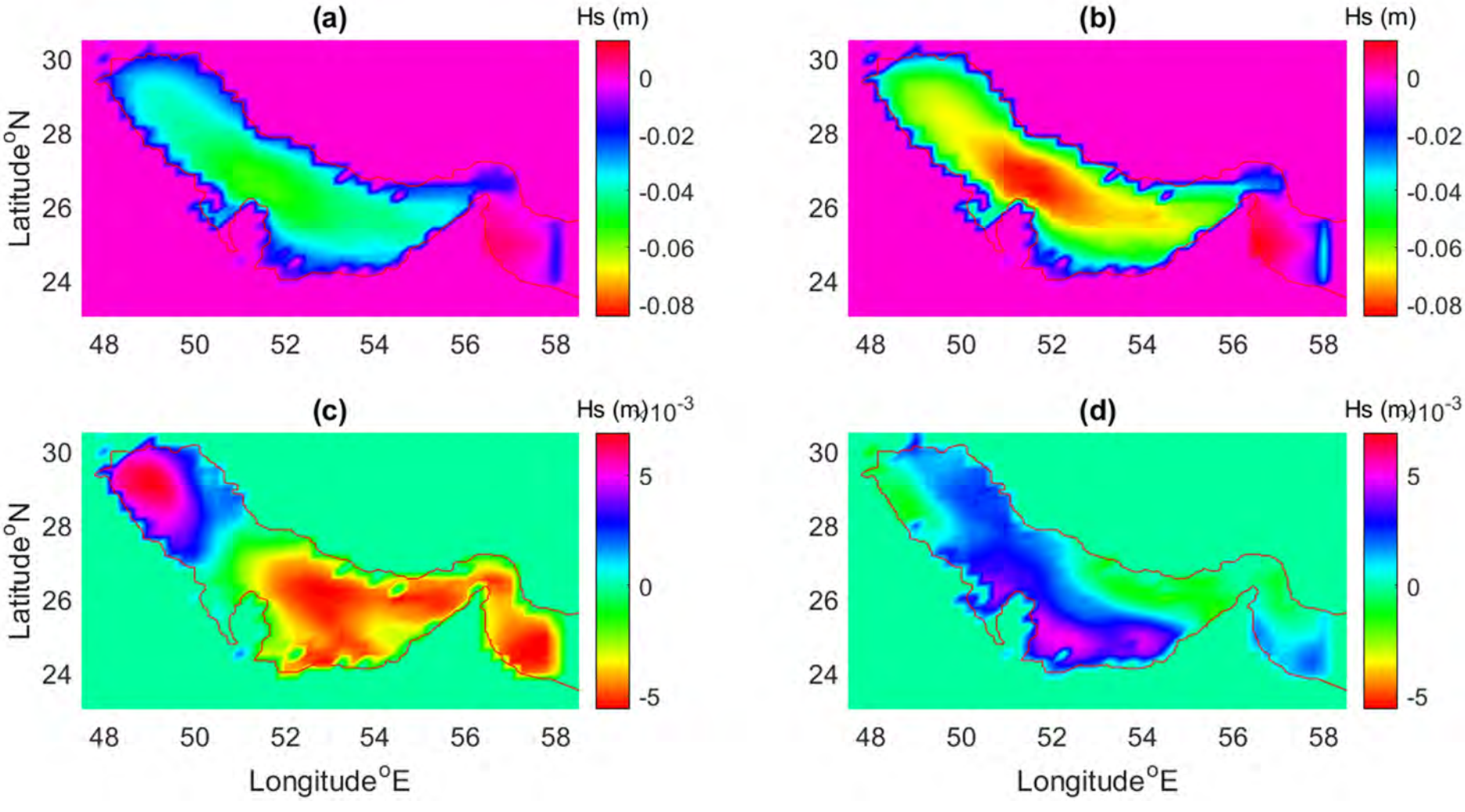
(a)
Hs (m)
0
-0.02
-0.04
-0.06
-0.08
30
28
26
24
Latitude°N
48
50
52
54
56
58
(b)
Hs (m)
0
-0.02
-0.04
-0.06
-0.08
(c)
Hs (m)
×10-3
5
0
-5
Longitude°E
(d)
Hs (m)
×10-3
5
0
-5
Longitude°E

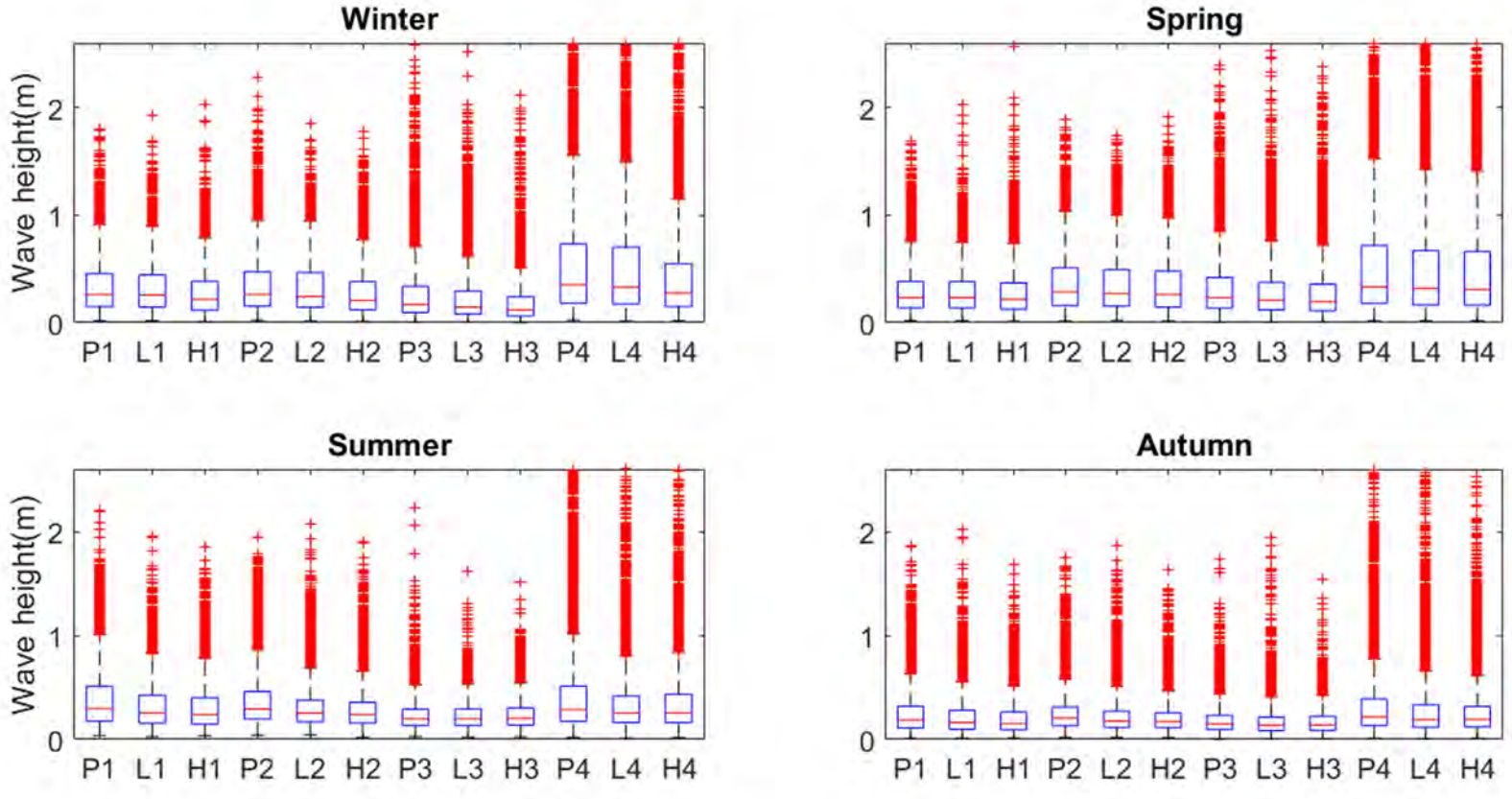
Winter
Spring
Summer
Autumn
Wave height(m)
0
1
2
P1 L1 H1 P2 L2 H2 P3 L3 H3 P4 L4 H4

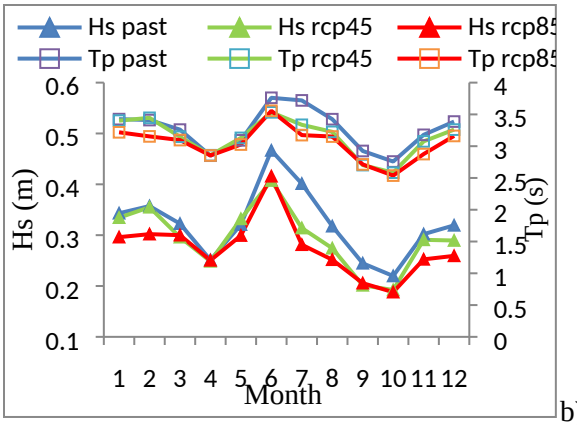
Hs past
Hs rcp45
Hs rcp85
Tp past
Tp rcp45
Tp rcp85
Hs (m)
Tp (s)
Month

a)

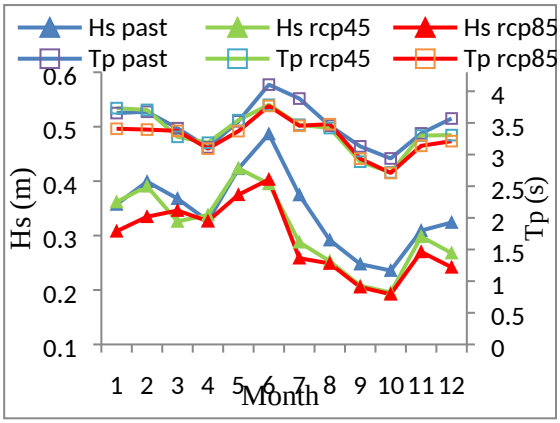
Hs past
Hs rcp45
Hs rcp85
Tp past
Tp rcp45
Tp rcp85
Hs (m)
Tp (s)
Month

b)

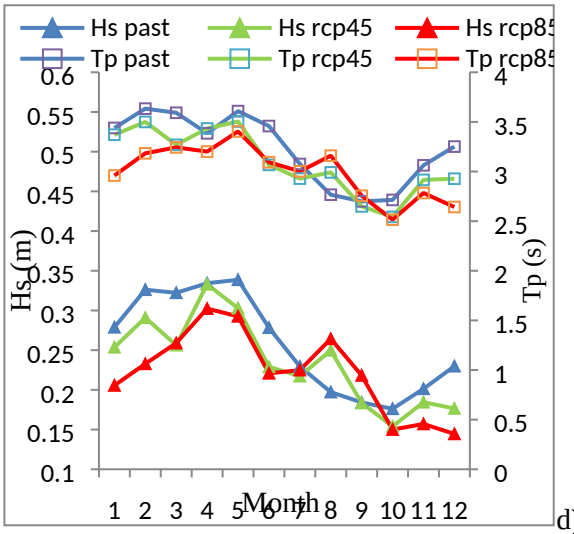
Hs past
Hs rcp45
Hs rcp85
Tp past
Tp rcp45
Tp rcp85
Hs (m)
Tp (s)
Month

c)

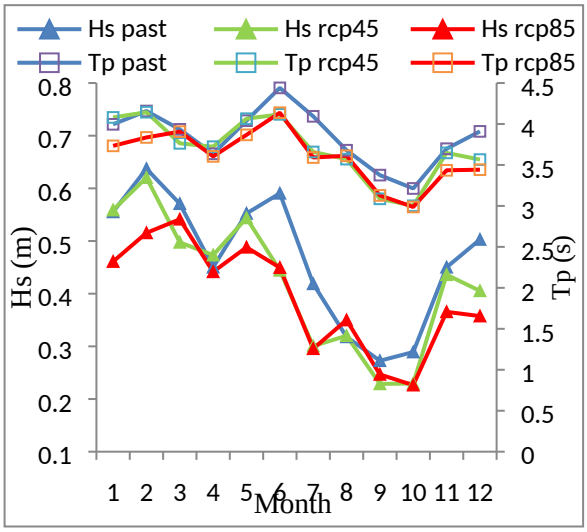
Hs past
Hs rcp45
Hs rcp85
Tp past
Tp rcp45
Tp rcp85
Hs (m)
Tp (s)
Month

d)